FLEXIBLE OBSTACLES IN RIVER AND FLOOD FLOWS: A LABORATORY STUDY

A dissertation submitted to The University of Manchester for the degree of Master of Engineering in the Faculty of Science and Engineering

2021

10762854

School of Mechanical, Aerospace and Civil Engineering

Table of Contents

ABSTRACT 7
DECLARATION 8
COPYRIGHT STATEMENT 8
ACKNOWLEDGEMENTS 9
NOTATION 10
1. INTRODUCTION 12
1.1. Problem justification 12
1.2. Project Aims and objectives 13
1.2.1. Aim 13
1.2.2. Objectives 13
1.3. Dissertation Scope 13
2. LITERATURE REVIEW 14
2.1. Floods 14
2.1.1. Vulnerability 14
2.1.2. Actions 15
2.2. Open Channel Flow 16
2.2.1. Uniform and non-uniform channel flow 17
2.2.2. Velocity distribution 17
2.2.3. Froude Number 18
2.2.4. Discharge Equations 19
2.2.5. Reynolds number 22
2.3. Open Channel Flow with obstacles 22
2.3.1. Drag Force – Isolated obstacle 22
2.3.2. Flexible bodies in flows 23
2.3.3. Mechanical properties of the obstacles 24
2.3.4. Drag in flexible bodies 25
2.3.5. Deformation of submerged flexible obstacles 28
2.3.6. Drag forces in obstacle array 29
2.4. Literature review Summary 31
3. METHODOLOGY AND PRELIMINARY TESTS 31
3.1. Modelling Approach 31
3.2. Equipment and Methodology 32

3.2.1. Flume 32
3.2.2. Flow Meter 33
3.2.3. Point gauge 34
3.2.4. Acoustic Doppler Velocimeter (ADV) 34
3.2.5. Strain Gauge 36
3.3. Channel depth 37
3.3.1. Method 37
3.3.2. Results 37
3.4. Channel velocity profile 38
3.4.1. Method 38
3.4.2. Results 38
3.5. Flow Rate and Mean Velocity 46
3.5.1. Method 46
3.5.2. Results 46
3.6. Obstacles 46
4. ISOLATED FLEXIBLE CYLINDERS 50
4.1. Forces on the Cylinders 50
4.1.1. Aim 50
4.1.2. Method 50
4.1.3. Results 54
4.2. Deformation of the Cylinders 59
4.2.1. Aim 59
4.2.2. Method 59
4.2.3. Results 62
5. DISCUSSION 64
5.1. Drag Forces 64
5.1.1. Relationship of Drag force with Velocity 64
5.1.2. Standard Deviation 65
5.2. Drag Coefficient 65
5.2.1. Drag Coefficient calculated from the experiments 65
5.2.2. Drag Coefficient from previous works 67
5.3. Variation in function of the Velocity and Reynolds number 69
5.4. Variation in function of the flexibility 70

6. CONCLUSIONS AND RECOMMENDATIONS 75
6.1. Conclusions 75
6.2. Recommendations 77
REFERENCES 79
APPENDIX 81

List of Tables

Table 1 the ten freshwater flood events with most people killed (Jonkman, 2005) 15
Table 2 Typical values of Manning's Coefficient (Chow, 1959) 21
Table 3 Velocity profile values in X direction 40
Table 4 Velocity profile values in Y direction 42
Table 5 Velocity profile values in Z direction 42
Table 6 Standard deviation - three directions and resultant 44
Table 7 Turbulence intensity along the height 45
Table 8 Rate flow and mean velocity for cases 1, 2 and 3 46
Table 9 Voltage output and force equivalent 55
Table 10 Force Standard deviation for the three type of obstacles 59
Table 11 Maximum deformation of cylinders 63
Table 12 Drag coefficient - Model 1 66
Table 13 Drag coefficient - Model 2 66
Table 14 relationship between CD and CD0 – Model 1 71
Table 15 Reconfiguration number - model 2 72

List of Figures

Figure 1 Percentage of people affected by type of disaster (CRED, 2015) 14
Figure 2 Percentage of deaths by type of disaster. (CRED, 2015) 15
Figure 3 Flexible obstacles in flood plain, man-made and vegetation 16
Figure 4 Open Channel sketch – longitudinal section / cross-section 17
Figure 5 Typical velocity profile 18
Figure 6 Wave propagation (Chaudhry, 2008) 19
Figure 7 Control volume for uniform flows 20
Figure 8 Main forces acting upon a flexible body 23
Figure 9 Tensile body and flexural body 24
Figure 10 Lateral rigidity of a cantilever beam 25
Figure 11 Obstacle height H in no-flow condition and height hv under flow conditions. 29
Figure 12 Laboratory Flume 32

Figure 13 Flow path along the flume 33
Figure 14 Rate totaliser 33
Figure 15 Flow path along the flume 33
Figure 16 Point gauge 34
Figure 17 Acoustic Doppler Velocimeter 35
Figure 18 ADV sensors 35
Figure 19 Strain gauge 36
Figure 20 Strain Gauge 37
Figure 21 Velocity measured by ADV at z=10mm 39
Figure 22 Velocity measured by ADV at z=155mm 39
Figure 23 Velocity profile m/s 40
Figure 24 Velocity profile V/Vm 41
Figure 25 Velocity profile in Y direction (m/s) 43
Figure 26 Velocity profile in Z direction (m/s) 43
Figure 27 Turbulence Intensity profile 45
Figure 28 tubes 47
Figure 29 tubes – sections 47
Figure 30 Plane view of single cylinder 49
Figure 31 Elevation of single cylinder 49
Figure 32 Force balance sketch - One side 50
Figure 33 Force measurement sketch 51
Figure 34 Force measuring - Case 1 52
Figure 35 Force measuring - Case 2 53
Figure 36 Force measuring - Case 3 53
Figure 37 voltage vs time 54
Figure 38 Force – voltage 55
Figure 39 Experiment case 1 Re=2736 / Experiment case 2 Re=4260 / Experiment case 3 Re=5508 56
Figure 40 Force measured in the case 1 on the Obstacle 1 White 57
Figure 41 Force measured in the case 3 on the Obstacle 1 White 57
Figure 42 Idealization of the problem 60
Figure 43 cylinder model 60
Figure 44 cylinder model - constrains 61
Figure 45 pressure distribution in cross-section 61
Figure 46 cylinder deformation 63
Figure 47 Force per unit area vs Velocity 64
Figure 48 Standard deviation vs Velocity 65
Figure 49 Relation of CD and Re (White, 1991) 67
Figure 50 Drag Coefficient vs Re (Cheng & Nguyen, 2011) 68
Figure 51 Cd as a function of Re according to CHANG & NGUYEN 69
Figure 52 Drag coefficient vs Re 69
Figure 53 Drag coefficient vs Re (Chapman, Wilson, & Gulliver, 2015) 70
Figure 54 Relationship α=CD/CD0 vs Cauchy Number 71
Figure 55 Relationship CD/CD0 vs Cauchy Number (Chapman, Wilson, & Gulliver, 2015) 72
Figure 56 Reconfiguration number vs Ca 73

Figure 57 Reconfiguration number vs Ca. Produced from (Whittaker, Wilson, & Aberle, 2015) 73
Figure 58 Drag coefficient vs EI - Cases 1, 2 and 3 74
Figure 59 Drag coefficient vs Re - Type of obstacle 75

ABSTRACT

Understanding how flexible bodies interact with flow is important in urban hydrology, river restoration, and flood mitigation. Several studies have demonstrated the influence on flow velocity turbulence; this effect can be applied for the flood control of channels and rivers. Flexible bodies, however, are known to behave differently than rigid ones due to deformation and interactions with turbulence, requiring additional investigation.

In this dissertation, drag forces for single flexible cylindrical obstacles were measured in a flume; the cylinders had the same material and size but with variable levels of flexibility under different flow conditions. The range of Reynolds Number, based on the cylinder diameter, was from 2000 to 6000. The tested obstacles had Cauchy numbers based on their flexural stiffness in the range of 10^{-3} to 10^{-2}.

Through two analytical models, the drag coefficients C_D were obtained, with values between 1.2 and 1.7, that agree with other authors for the same range of Re and Ca.

We found that the ratio of the calculated drag coefficient of C_D to the drag coefficient of a stiff element C_{D0} is approximately 1 for our range of Cauchy Number Ca, this ratio decreases slightly to around 0.97 for the highest Ca, that is the most flexible obstacle.

Furthermore, we found a high dependence of the drag coefficient on the Reynolds number, as well as the relationship between the drag forces and velocity. Additionally, we observed higher values of standard deviation in the measured force when the velocity increases. This suggests that in further studies, the effect of the vibration in the obstacle on the drag coefficient, as well as the effect of higher Reynolds number and Cauchy number, should be considered.

DECLARATION

No portion of the work referred to in the thesis has been submitted in support of an application for another degree or qualification of this or any other university or other institute of learning.

COPYRIGHT STATEMENT

i. The author of this dissertation (including any appendices and/or schedules to this dissertation) owns certain copyright or related rights in it (the "Copyright") and s/he has given The University of Manchester certain rights to use such Copyright, including for administrative purposes.

ii. Copies of this dissertation, either in full or in extracts and whether in hard or electronic copy, may be made only in accordance with the Copyright, Designs and Patents Act 1988 (as amended) and regulations issued under it or, where appropriate, in accordance with licensing agreements which the University has entered into. This page must form part of any such copies made.

iii. The ownership of certain Copyright, patents, designs, trademarks and other intellectual property (the "Intellectual Property") and any reproductions of copyright works in the dissertation, for example graphs and tables ("Reproductions"), which may be described in this dissertation, may not be owned by the author and may be owned by third parties. Such Intellectual Property and Reproductions cannot and must not be made available for use without the prior written permission of the owner(s) of the relevant Intellectual Property and/or Reproductions.

iv. Further information on the conditions under which disclosure, publication and commercialisation of this dissertation, the Copyright and any Intellectual Property and/or Reproductions described in it may take place is available in the University IP Policy, in any relevant Dissertation restriction declarations deposited in the University Library, and The University Library's regulations.

ACKNOWLEDGEMENTS

I would like to express my deepest gratitude to my supervisor, Dr Gregory Lane-Serff, for his invaluable supervision and helpful advice, comments and suggestions throughout the process of this dissertation.

I would like to express sincere thanks for the financial support offered by the Peruvian scholarship program PRONABEC, for betting on a better education and opportunities for more Peruvians.

Finally, the greatest thanks for being my encouragement and strength to my source of inspiration Patricia and Jorge, to my supportive and beloved Julio, and to my dearest Mayra, Jorge and Aldo.

NOTATION

A	Flow cross-section area
A_p	projected area in the direction of the flow
A_{p0}	projected area for no flow conditions
B	Channel width
C	Chezy constant
D	Diameter of obstacle
C_D	Drag coefficient
C_{D0}	Drag coefficient of a rigid body
c_f	skin-friction coefficient,
E	Modulus of Elasticity
f	friction or Darcy-Weisbach factor
F_D	Drag force
f_D	Drag force per unit area
$\boldsymbol{F}_r$	Froude Number
g	gap between obstacle and flume base
H	flow depth
L	Characteristic length
n	Manning´s coefficient
P	Wetted Perimeter
Q	Flow rate
R	Hydraulic radius
Re	Reynolds number
Rn	Reconfiguration number
S_0	Slope
S_f	Slope of energy grade line.
S_R	Slenderness ratio
ν	kinematic viscosity

V	Velocity
Vm	Mean velocity
Vol	Volume of the obstacle
y	flow depth
α	Ratio of C_D and C_{D0}
δ	Boundary layer depth
λ	Solid Volume Fraction
ψ	Vogel exponent

1. INTRODUCTION

1.1. Problem justification

Floods affect people around the world every year, with a more serious impact in those countries with poor urban planning and with a lack of technical knowledge to mitigate its damage. A flood is a type of disaster that affects most people around the world; some aspects that increase the vulnerabilities of low-income cities in developing countries are urbanization, population congestion, intensification of settlement sites, and poverty (Parker, 2014).

According to the Centre for Research on the Epidemiology of Disasters (CRED), data studied in 2014 shows that while Earthquakes are typically more deadly than other disasters, in 2013 hydrological disasters caused 71% of the deaths (CRED, 2015).

Furthermore, floods expose people, most particularly children, to respiratory infections, skin allergies, and many forms of gastro-intestinal ailments; many poor residents face the risk of mosquito bites that could be vectors of infectious diseases; commuters put them at risk of falling into open manholes, unmarked constructions diggings and open canals; and the list of flood consequences goes further (Parker, 2014).

Flood mitigation should be planned as a complete and integral system where it is necessary to carry out in depth technical evaluation of flood hazards, the performance of the existing flood protection systems, the implementation of structures along the basin, the maintenance standards, and other aspects.

Riparian forests have been extensively promoted for flood protection, sediment management, and erosion control projects. (Ishikawa, Mizuhara, & Ashida, 2000); nevertheless, because of deformation and interactions with turbulence, flexible bodies are known to behave differently than rigid bodies, demanding further consideration. Every aspect of flood management requires an understanding of how vegetation and other structures interacts with the flow. Several studies have demonstrated the influence on flow velocity turbulence (Stephan & Gutknecht, 2002), and lodging velocities of flexible obstacle, as well as its influence in surface wave forces; this effect on the behaviour of flows can be applied for the control of channels and rivers as part of integral flood defence projects.

1.2. Project Aims and objectives

1.2.1. Aim

The main aim of this dissertation work is to carry out experimental models to study the drag on flexible obstacles in open channel flows. The flexible obstacles are cylindrical elements of different sections that represent certain types of plants and man-made obstacles.

1.2.2. Objectives

To investigate the behaviour of obstacles, we must first establish the features of the flow in which they are placed; hence, one of the aims is to conduct preliminary tests that allow defining of the hydraulic dimensions, flow rates, and flow velocities of each scenario to be studied.

The literature proposes different models for the study of drag forces on flexible obstacles, each one is adapted to certain scenarios depending on which of the study characteristics are variable and which are constant; therefore, our objective is to study two models and discuss how the parameters found experimentally are related to the results obtained in previous research works.

Our last objective is to evaluate how the drag forces vary as a function of the properties of the element itself and as a function of the properties of the flow. These results shown through graphs and tables to allow us to discuss the relationships, coincidences and disagreements with previous works in similar conditions; as well as to determine whether it is possible to extrapolate our model to similar scenarios.

1.3. Dissertation Scope

The body of this dissertation is divided into 6 chapters. In the next chapter, we will review flood impacts and the basic concepts of open channels and uniform flows, as well as the principles necessary for the study of forces and drag coefficients. In the third chapter, we will focus on the preliminary experiments, reviewing the equipment we use and the methodology to follow. In Chapter 4, the analysis will be focused on flexible obstacles, both in obtaining the drag forces through experiments, and the analysis of finite elements to determine the deformations. Following this, we will discuss the results obtained in the previous chapters and finally, we will issue the conclusions of the work.

2. LITERATURE REVIEW

2.1. Floods

Floods are natural and frequent occurrences, Hays (1981) claimed that “the natural function of a flood plain is to carry away excess water in time of flood”, he also said however that “they become a hazard when man competes for the use of flood plains.” (Hays, 1981)

2.1.1. Vulnerability

Alexander identifies the types of vulnerability according to the social context, and other factors like total vulnerability (Alexander, 1997), economic vulnerability, technological vulnerability, newly generated vulnerability. Blaikie presents a model of the socio-economic and political underpinnings of vulnerability to disaster (Blaikie, 1985). These models agree that floods affect people's lives on a large scale, affecting different aspects of our lives.

The Centre for Research on the Epidemiology of Disasters (CRED) divulges the percentage of people affected and people death by type of disaster obtained during the years 1994 – 2013. (CRED, 2015)

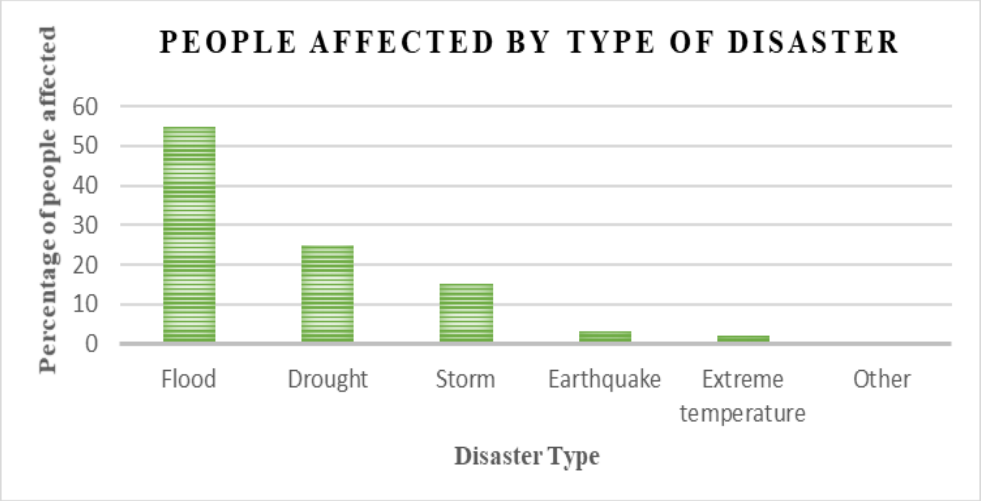

Figure 1 Percentage of people affected by type of disaster (CRED, 2015)

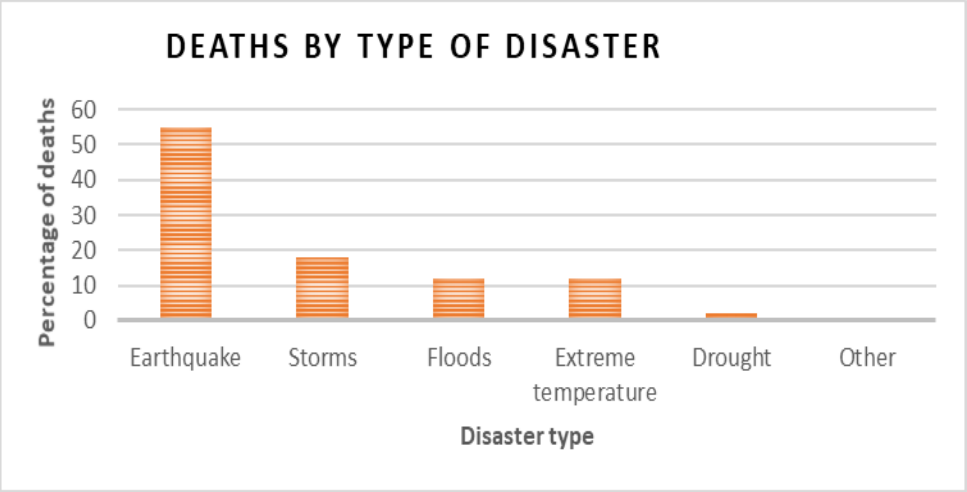

Figure 2 Percentage of deaths by type of disaster. (CRED, 2015)

The statistics are even more discouraging when we look more closely at the events with more fatalities. Jonkman compiles the five floods with most persons killed, shown in Table 1 (Jonkman, 2005)

Table 1 the ten freshwater flood events with most people killed (Jonkman, 2005)

Country	Year	Killed	Total affected
Venezuela	1999	30,000	483,635
Afghanistan	1988	6345	166,831
China, P. Rep	1980	6200	67,000
India	1978	3800	32,000,000
China, P. Rep	1998	3656	238,973,000

2.1.2. Actions

Various authors have investigated the effect of flexible obstacles such as vegetation on how they affect the characteristics of flows in rivers and channels.

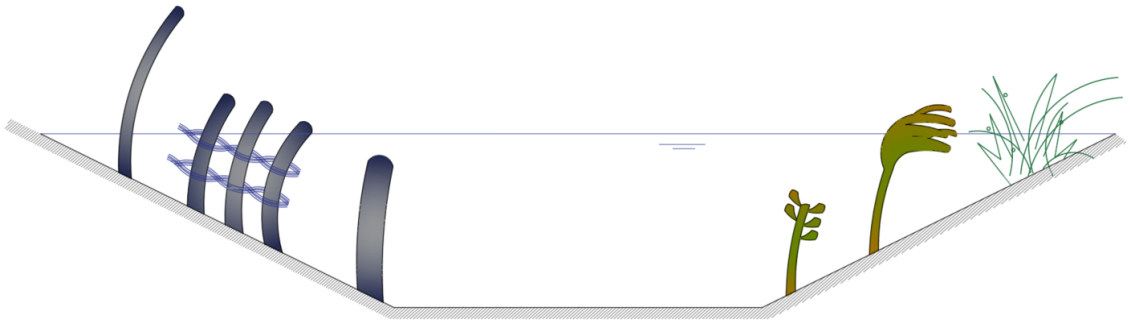

Figure 3 Flexible obstacles in flood plain, man-made and vegetation

The reforestation and implementation of other flexible structures in control methods could increase the river channel's resistance and help to mitigate floods (Loboda, Karpinski, & Bialik, 2018).

In the case of flexible vegetation, such as aquatic vegetation, stem reconfiguration is essential since it may minimise roughness and therefore greatly impact flow velocity when compared to rigid vegetation. Errico et al. (2018) proved that the presence of vegetation has a significant impact on velocity distribution. The presence of thick canopies on the channel sides resulted in flow concentration, with a considerable increase in flow velocity in the centre, open area in full-vegetated circumstances. (Errico, et al., 2018)

Darby (1999) in one study about riparian vegetation and how it affects flow resistance and flood potential, found that flood elevation discharge differs markedly according to type and extent of vegetation, as well as variation in the stem properties themselves (Darby, 1999).

Parameters that can be predicted from the physical characteristics of the flexible obstacles are still needed. The importance of flood management through the reforestation of rivers and canals, as well as the implementation of man-made elements, leads us to study models that allow us to predict mainly the forces to which these elements will be subjected as well as how susceptible they are to variations in certain characteristics of the flow and its flexibility.

2.2. Open Channel Flow

Open-channel flows are ones that are not completely contained within rigid limits; a portion of the flow is in contract with nothing but air (Chaudhry, 2008).

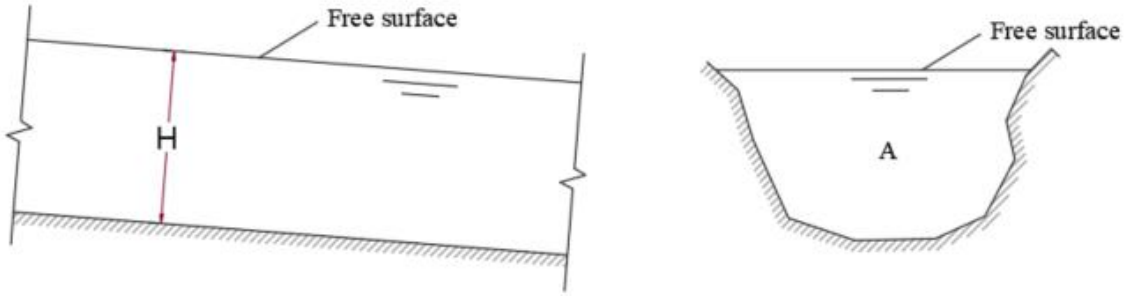

Figure 4 Open Channel sketch – longitudinal section / cross-section

2.2.1. Uniform and non-uniform channel flow

In general, uniform flow is defined as an open-channel flow in which all variables are constant in an instant, namely the discharge, depth, width, and mean velocity (Hamill, 2011) within a particular channel length. If the channel is long and prismatic, the flow will accelerate or decelerate for a distance until the accelerating and resistive forces balance. The flow velocity and depth stay constant from that point forward. (Chaudhry, 2008)

Numerous channels are built to transport fluids at a constant depth throughout their length. Irrigation canals are often uniform in depth and cross-section across long distances. Natural channels, like rivers and streams, are rarely uniform, yet assuming uniform flow can frequently provide a good estimation of the flow rate. (Munson, 2009)

2.2.2. Velocity distribution

The velocity of the flow in a channel section changes from point to point. This is due to shear stress at the bottom and sides of the channel, as well as the presence of a free surface. (Chaudhry, 2008). A fluid flow, in general, is a three-dimensional, time-dependent phenomenon $V = V(x, y, z, t)$; all three Cartesian coordinate directions may have components in the flow velocity. However, in many cases, simplifying assumptions can be made that allow for a far clearer comprehension of the problem without sacrificing needed precision. The components of vertical and transverse directions are neglected since they are typically small. As a result, just the flow velocity in the flow direction is considered in this study $V = V(x, t)$.

Figure 5 depicts a typical change of velocity with depth. The velocity component changes as we get further away from the free surface.

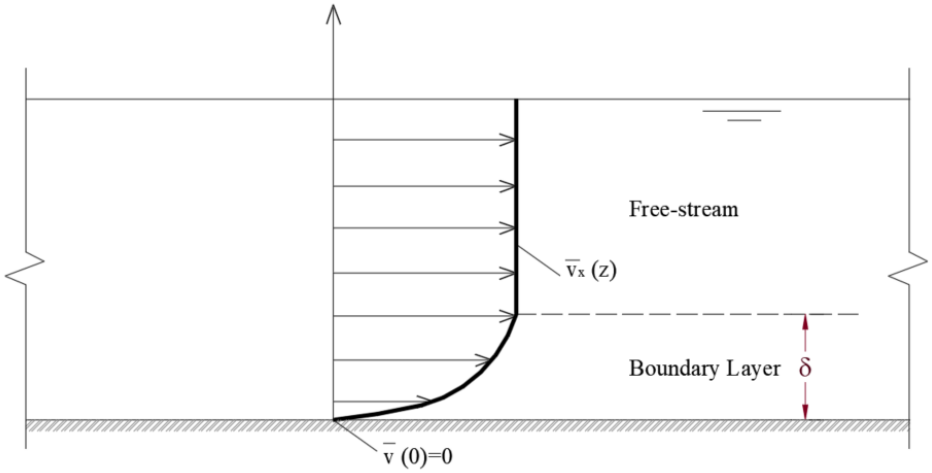

Figure 5 Typical velocity profile

2.2.3. Froude Number

If the flow velocity is equivalent to the velocity of a small-amplitude gravity wave, the flow is said to be critical. If the flow velocity is less than the critical velocity, the flow is called subcritical flow; if the flow velocity is greater than the critical velocity, the flow is called supercritical flow. The Froude number, Fr, is equal to the ratio of inertial and gravitational forces:

$$\boldsymbol{F}r = \frac{V}{\sqrt{gH}} \qquad (1)$$

For rectangular channels where H= flow depth, depending on the respective magnitudes of V and c, three distinct flow conditions for the propagation of a disturbance are conceivable. When V< c, or Fr < 1, the flow is subcritical, when V>c, or Fr > 1 it is supercritical; For the special case of V=c, or Fr=1 the upstream propagating wave remains stationary, and the flow is called critical. (Hamill, 2011)

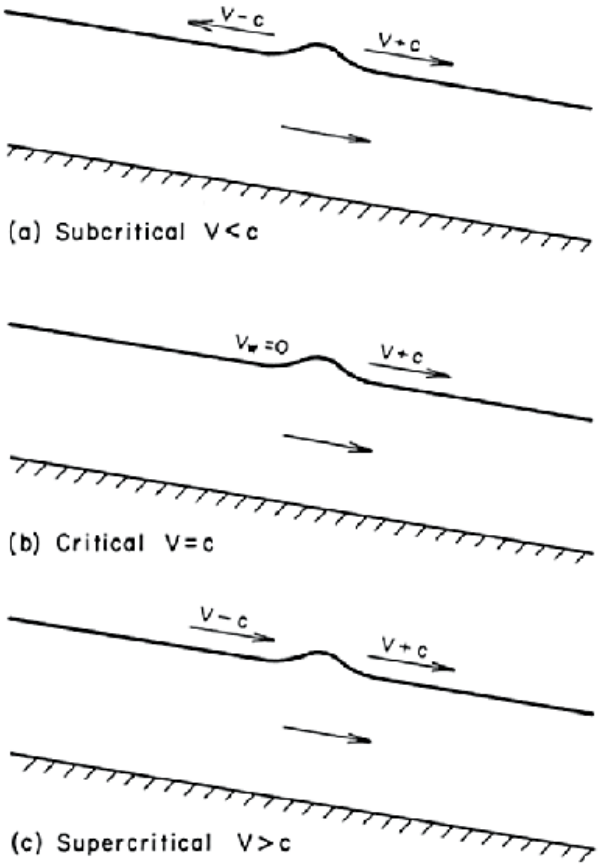

Figure 6 Wave propagation (Chaudhry, 2008)

2.2.4. Discharge Equations

Chezy equation

To derive the Chezy equation, researchers made the following assumptions: The flow is steady; the slope of the channel bottom is small where and the channel is prismatic. (Chaudhry, 2008), Figure 7 shows the forces acting in a given length of a channel.

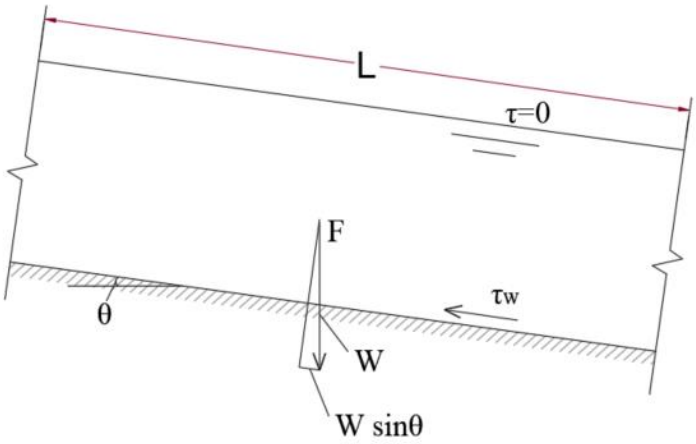

Figure 7 Control volume for uniform flows

The term W sinθ refers to the component of the fluid weight that acts down the slope, while τ_wPL refers to the shear force on the fluid that acts up the slope because of the water's contact with the wetted perimeter of the channel. (Munson, 2009)

Since there is no acceleration of the fluid, the system is controlled by a simple balance of the forces in the direction of the flow, thus $\sum F_x = 0$, then

$$\tau_w \mathrm{PL} = \mathrm{W}\sin\theta \tag{2}$$

$$\tau_w = \frac{\mathrm{W}S_0}{PL} = \frac{\gamma ALS_0}{PL} \tag{3}$$

In terms of the hydraulic radius R defined as $R = A/P$, A is the flow cross-section and P is the wetted perimeter, equation (3) becomes:

$$\tau_w = \gamma R S_0 \tag{4}$$

A. Chezy (1718–1798) obtained that for non-uniform flows:

$$V = C\sqrt{RS_f} \tag{5}$$

while for uniform flows:

$$V = C\sqrt{RS_o} \tag{6}$$

where C = Chezy constant and the slope of the energy grade line, S_f, is used for nonuniform flow, while the slope of the channel floor S_0 is used for uniform flow, (which has the same

value as the slope of the water surface). The Chezy constant and the Darcy-Weisbach friction factor are given respectively by the following equations:

$$C = \frac{2g}{c_f} \tag{7}$$

$$f = 4\,cf \tag{8}$$

Where c_f is a dimensionless skin-friction coefficient.

Manning Coefficient

The value of the Manning coefficient *n* is influenced by surface roughness, vegetation, and channel irregularity, as well as stage, scour and deposition; and is obtained from experiments.

Uniform flow in an open channel is obtained from the Manning equation written as:

$$V = \frac{1}{n} R^{2/3} S_0{}^{1/2} \tag{9}$$

Equation (9) is valid for SI units, i.e., V is in m/s, and R is in m (Munson, 2009). Some typical values of *n* are shown in the table below:

Table 2 Typical values of Manning's Coefficient (Chow, 1959)

Material	***n***
Steel	0.012
Cast iron	0.013
Corrugated metal	0.025
Lucite	0.009
Glass	0.010
Cement	0.011
Concrete	0.013
Wood	0.012
Clay	0.013
Brickwork	0.013
Gunite	0.019
Masonry	0.025
Rock cuts	0.035

Natural streams – clean and straight	0.030
Natural streams – bottom: gravel, cobbles.	0.040
Natural streams – bottom: cobbles with boulders	0.050

2.2.5. Reynolds number

Reynolds number is used to identify whether the flow is laminar or turbulent. If the liquid particles appear to move in distinct smooth routes and the flow appears to be a movement of thin layers on top of each other, the flow is called laminar flow. In turbulent flow, the liquid particles travel along uneven pathways that are not fixed in time or space.

The Reynolds number is the ratio of viscous and inertial forces; if viscous forces prevail, the flow is laminar; if inertial forces dominate, the flow is turbulent.

$$Re = \frac{V_m L}{\nu} \tag{10}$$

where Re = Reynolds number; V_m = mean flow velocity; L = a characteristic length; and ν = kinematic viscosity of the liquid.

2.3. Open Channel Flow with obstacles

2.3.1. Drag Force – Isolated obstacle

Due to the interaction between a body and a moving fluid surrounding it, the body immersed in the fluid experiences a resulting force. This effect can be given in terms of the forces at the fluid–body interface. (Munson, 2009)

The distribution of shear stress and pressure over the surface of the body is often difficult to obtain; however, the resultant force is commonly more useful, this force is called drag. The most common method is to define the dimensionless drag coefficient and estimate its value using either a simplified analysis or a simulation.

$$F_D = C_D \frac{1}{2} \rho V^2 A_p \tag{11}$$

where *Ap* is the frontal area of the obstacle, in this study *Ap=DxH*

$$F_D = C_D \frac{1}{2} \rho V^2 DH \tag{12}$$

where F_D is the drag force, C_D is a drag coefficient, ρ is the fluid density.

2.3.2. Flexible bodies in flows

Flexible bodies are understood to behave differently from rigid bodies because of deformation. Characterizing the deformation and flexibility of an object can be achieved with parameters such as the modulus of elasticity, also known as Young's Modulus, E (Hibbeler, 2011).

Figure 8 shows the forces acting on the flexible body in a given flow condition, F_D is the drag force, Fb is the buoyancy force, Fg is the gravity force and Fr is the resultant force (Loboda, Karpinski, & Bialik, 2018)

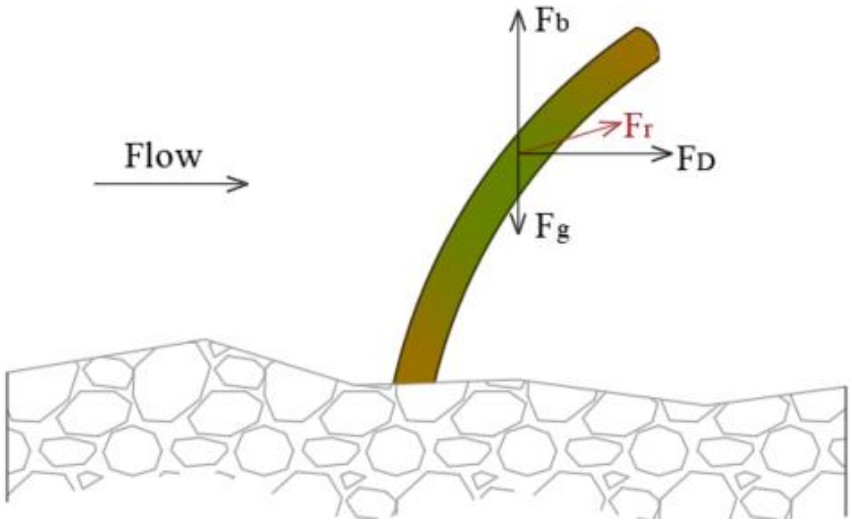

Figure 8 Main forces acting upon a flexible body

As displayed on Figure 9, there are two types of bodies according to how they adjust to specific flow conditions: tensile elements, e.g., plants like periphyton, and bending elements e.g., stream bank plants, man-made obstacles (Nikora, 2010). It is the flexural stiffness of the element, which is one of the most significant mechanical characteristics that impacts the fluid velocity by changing the drag force and the rate of mass flux (Albayrak, Nikora, Miler, & O'Hare, 2011).

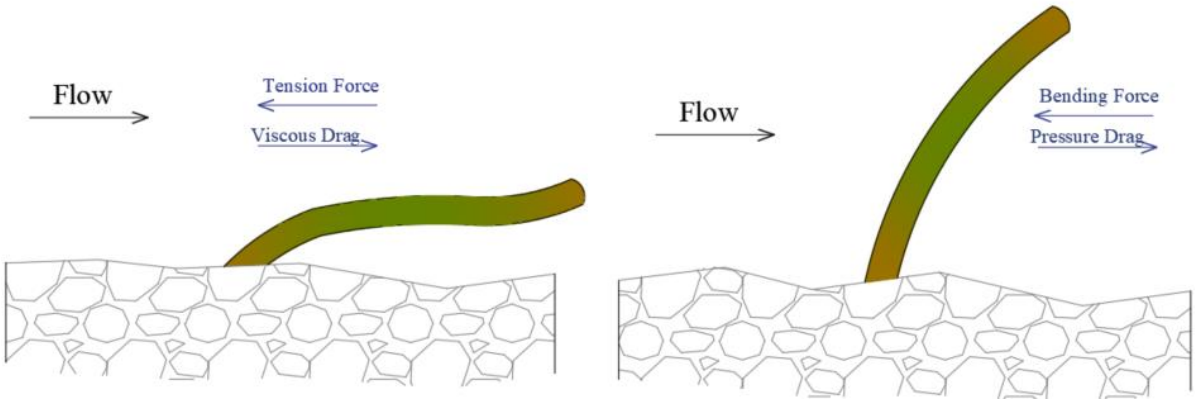

Figure 9 Tensile body and flexural body

According to Nikora, elements with high flexural rigidity is primarily susceptible to pressure drag, whereas elements with low flexural rigidity are vulnerable to viscous skin friction following the flow (Nikora, 2010).

2.3.3. Mechanical properties of the obstacles

The samples tested in the present study tend to be bending elements, therefore we study in more detail the mechanical properties of a beam-type bending element. Since the degree of flexibility of the obstacle is the inverse of its stiffness, this will depend on its geometry. For cylinder bodies with the cross-section as a ring, we have:

- Area of the cross-section

$$A = \pi(R^2 - r^2) \tag{13}$$

- Second moment of area

$$I = \frac{1}{2}\pi(R^4 - r^4) \tag{14}$$

- Stiffness

  Bending stiffness for a cantilever beam with distributed load

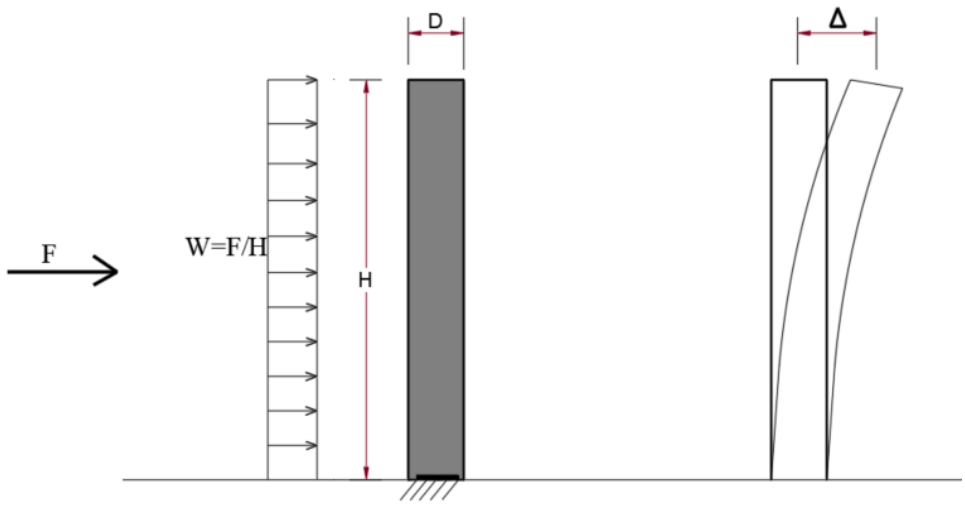

Figure 10 Lateral rigidity of a cantilever beam

$$K = \frac{Load}{Displacement} \tag{15}$$

$$k = \frac{8EI}{H^4} \tag{16}$$

2.3.4. Drag in flexible bodies

In the present dissertation work, we verify two models proposed by different authors, one of them is the one proposed in the research by Chapman, Wilson and Gulliver (2015), and the second one proposed by Whittaker, Wilson and Aberle (2015). Both models relate the drag forces with the degree of flexibility of the elements, but with different factors and concepts that are described below.

Vogel, in his research in 1984 and 1989, relates the drag force and the velocity, incorporating an exponent ψ. The author claimed that ψ is the exponent by which the velocity must be raised in order to be directly proportional to the drag coefficient or the drag divided by the square of the flow velocity (Vogel, 1989).

$$\frac{F_D}{V^2} \propto V^{\Psi} \tag{17}$$

$$then, F_D \propto V^{\Psi+2} \tag{18}$$

The value of the Vogel exponent is directly connected to the rate at which the projected area and drag coefficient decrease with increasing flow velocity, as shown by Equations (17) and (11) (Whittaker, Wilson, & Aberle, 2015).

Model 1

Model 1 (Chapman, Wilson, & Gulliver, 2015) is based on the drag force general formula and incorporates two parameters that depend on the ratio of projected areas A_p and A_{p0} (with and without flow conditions) β.

$$F = \frac{1}{2}\rho C_{D0} A_p V^2 \tag{19}$$

$$\beta = \frac{A_p}{A_{p0}} \tag{20}$$

$$F_F = \frac{1}{2}\rho C_D \beta V^2 \tag{21}$$

where C_D is the drag coefficient for a flexible element and C_{D0} is the drag coefficient for a rigid obstacle with the same characteristics.

$$C_D = C_{D0}\alpha \tag{22}$$

$$\alpha = (\frac{V_m}{V_x})^x \tag{23}$$

where the parameter α relates the drag C_D and C_{D0}. This parameter is defined as the ratio of the velocity of the experiment and a minimum referential velocity V_x to the x exponent. (Chapman, Wilson, & Gulliver, 2015). The exponent x is studied by different authors to characterize several types of obstacles, in some cases, species of vegetation, as did (Aberle & Järvelä, 2013) .

Cauchy number is also known as the ratio of the dynamic pressure to the modulus of elasticity.

$$C_a = \rho {V_m}^2 / E \tag{24}$$

where E is the Young's Modulus of the material. C_a must be scaled for obstacles using a slenderness number (S_R), a property of the obstacle, equal to the ratio of the maximum to the minimum dimension of the section of the obstruction that faces the flow. (Langre, 2008). Transverse loadings on slender beams are proportional to S_R^3 (the slenderness number of the obstruction), resulting in the C_{aS} shown in equation (25) (Chapman, Wilson, & Gulliver, 2015)

$$C_{aS} = (\rho {V_m}^2/E){S_R}^3 \tag{25}$$

Model 2

Whittaker provided a drag force model that uses the Cauchy number for the reconfiguration of flexible bodies. (Whittaker, Wilson, & Aberle, 2015)

$$F = \frac{1}{2}\,\rho K\,(\frac{\rho {V_m}^2 V_{ol} H}{EI})^{\Psi/2}\,{V_m}^2 \tag{26}$$

Where K is the combined C_dA_p value at low velocities where the obstacle is considered to behave like a rigid body; V_{ol} and EI denote the obstacle volume and flexural stiffness, respectively, whereas the terms within the parentheses denote the Cauchy number Ca. Through the ratio of inertial and elastic forces, the Cauchy number measures the flexibility of objects in a fluid flow.

$$Ca = \frac{\rho {V_m}^2 A_{po} H^2}{EI} \tag{27}$$

Reconfiguration Factor

Whittaker set the effect of reconfiguration is quantified by a dimensionless number R that compares the observed drag force to that of a comparable rigid object with the same shape. (Whittaker, Wilson, & Aberle, 2015)

$$R = \frac{2F}{\rho C_{D0} A_{p0} V^2} \tag{28}$$

Based on Vogel's original premise that the relationship between R and Ca follows a power law, the power to which the Cauchy number is increased is equal to half the Vogel exponent

(ψ/2). As a result, the variation in the typical drag coefficient with velocity may be characterised as follows:

$$C_D A_p = C_{D0} A_{p0} Ca^{\psi/2} \tag{29}$$

Whittaker et.al derived the new 'Cauchy model' for estimating the hydrodynamic drag forces applied on flexible vegetation by replacing the characteristic drag coefficient in Equation (11) with the relationship given in Equation (29): (Whittaker, Wilson, & Aberle, 2015)

$$F = \frac{1}{2} \rho C_{D0} A_{p0} Ca^{\Psi/2} V^2 \tag{30}$$

2.3.5. Deformation of submerged flexible obstacles

The element is assumed to be:

- A cylindrical cantilever beam.
- Material properties are homogeneous and isotropic
- The deformation is causing by bending only.

The bending stiffness (El) will be constant across the length of the beam in most cases. If this is the case, the equilibrium equations can be arranged into the three equations below: (Hibbeler, 2011)

$$EI \frac{d^4 v}{dx^4} = w(x) \tag{31}$$

$$EI \frac{d^3 v}{dx^3} = V(x) \tag{32}$$

$$EI \frac{d^2 v}{dx^2} = M(x) \tag{33}$$

Solving any of these equations requires successive integrations to obtain the deflection v of the elastic curve. The constants of integration are found by evaluating the functions for the shear force, moment, slope, or displacement at a given location on the beam when the value of the function is known when equations (31), (32), or (33), are solved. These values are called boundary conditions. (Hibbeler, 2011)

Now, for this case, it is also assumed that the obstacle is subjected to uniformly distributed hydrodynamic load; then, the element bending can be calculated by iterating the following equation:

$$\frac{ds}{dy} = [1 - \left(\frac{F_D}{2EI}\right)^2 \left(\frac{y^3}{3h_v} - y^2 + h_v y\right)^2]^{-0.5} \qquad (34)$$

where s is the curvilinear abscissa measured from the stem's bottom and hv is the stem's height under hydrodynamic force (Pasquino, et al., 2018), as shown schematically in Figure 11.

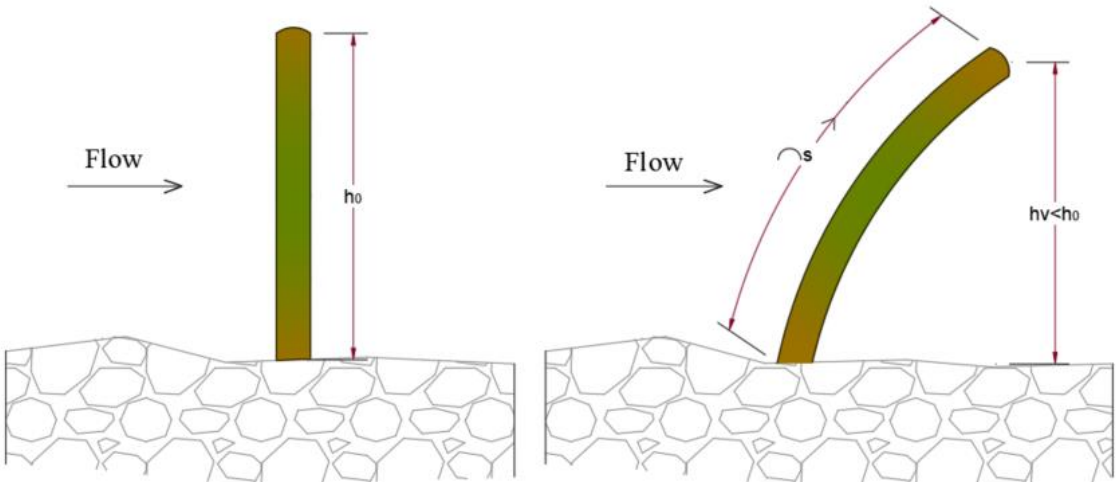

Figure 11 Obstacle height H in no-flow condition and height hv under flow conditions.

As input parameters, the algorithm applied by Stone and Pasquino needs an estimate of the obstacle drag force (F_D), the modulus of elasticity (E) of the obstacle, the nonstreamlined height (h_0), and the diameter of the element (D) (Stone, et al., 2011), (Pasquino, et al., 2018).

2.3.6. Drag forces in obstacle array

In this section we observe the influence of the of the obstacles array on the channel flow. Although the experimental work will focus on single obstacles, it is convenient to mention how the quantity and distribution of the elements influence the drag forces.

Solid Volume Fraction

One of the most common ways to relate the obstacles density with drag forces is through Solid Volume Fraction. According to (Tanino & Nepf, 2008), the solid volume fraction, λ is defined as the ratio of the volume occupied by simulated vegetation to the total volume occupied by the vegetation and water within the array. For uniform flow through an array of emergent circular cylinders, in a rectangular channel, this can be written as:

$$\lambda = \frac{\pi}{4}\frac{ND^2}{BL_n} \tag{35}$$

where N is the total number of cylinders within the array, D is the cylinder diameter, B is the channel width and L_n is the length of the array.

Reynolds number

Reynolds number in terms of the cylinder width and array-averaged velocity: (Tanino & Nepf, 2008)

$$Re_n = \frac{V_n D}{v} \tag{36}$$

$$V_n = \frac{V}{(1-\lambda)} \tag{37}$$

Hydraulic Radius

When assessing obstacles' resistance, the frontal area of the element must be considered rather than the complete wetted area. Consequently, the obstacle hydraulic radius, r_n is the ratio of the volume of water to the frontal area of the obstacles (Cheng & Nguyen, 2011). This gives the obstacle hydraulic radius for an array of circular cylinders:

$$r_n = \frac{\pi}{4}\frac{(1-\lambda)}{\lambda}D \tag{38}$$

Drag force

The total drag force exerted on an array of circular or square cylinders is the product of the mean drag force per cylinder and the number of cylinders. The array-averaged drag coefficient (Eq. (35)) can be used to calculate the mean drag force per cylinder. The total

cylinder drag can be equated with the down-slope component of the weight water if the drag on the flume walls is ignored and the flow is uniform. For circular and square cylinders (Robertson, 2016):

$$C_{Dn} = \frac{2(1-\lambda)gBL_nS}{NDV_m{}^2} = \frac{2gr_nS}{V_m{}^2} \quad (39)$$

2.4. Literature review Summary

In this chapter, we have reviewed different sources that allow us to examine in more detail the continuously latent problem of floods, our vulnerability to them and how we can use the current knowledge in the use of flexible structures as an option for their control.

Afterwards, we have reviewed the essential concepts about open channels and all the features that we need for the analysis of the drag forces that we collect in the laboratory.

The authors emphasize that the behaviour of flexible elements depends on the Reynolds number and therefore on the flow velocity, as well as its degree of flexibility. Various researchers propose different models to predict this behaviour; it is essential to identify the variables that we know and can obtain or approximate, as well as the characteristics of the elements to choose the model that best suits each situation. Thus, the experiments will aim to establish the accuracy of the proposed models.

3. METHODOLOGY AND PRELIMINARY TESTS

3.1. Modelling Approach

Experiments can be carried out in natural channels in the field or in the laboratory on genuine patches of plants. These tests can be used to estimate resistance coefficients, The following variables may affect the experiment:

- Geometry of the obstacle.
- Degree of flexibility of the obstacle.
- The distribution of the obstacles.
- Channel geometry.
- Characteristics of the flow.

In order to avoid having a large number of variables, the model can be simplified using simple geometries of the obstacles, in a laboratory flume with constant cross-section. In the present study, we tested three polyamide tubes, each one with a different cross-section, therefore different stiffness. We also repeated the tests under three different flow conditions. Channel geometry is constant for all the cases of this study. For this purpose, the flume equipment of the hydraulic laboratory of the University of Manchester will be used, the characteristics of this flume are detailed in the following section.

3.2. Equipment and Methodology

3.2.1. Flume

Laboratory experiments were performed in a re-circulating flume in the hydraulics laboratory in the Pariser building at the University of Manchester. The dimensions of the flume are 5m length, and 0.30mx0.30m of cross-section. The material of the walls is glass.

Figure 12 Laboratory Flume

The water path is shown in Figure 13 For the course of each experiment, water circulates continuously across the flume. The pump is turned off after each experiment, and the water in the test area empties into the tank below via the outlet.

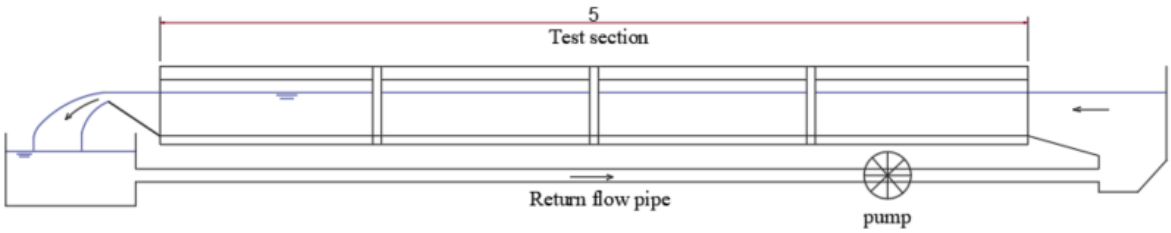

Figure 13 Flow path along the flume

3.2.2. Flow Meter

The flowmeter is a digital instrument that shows the total amount of flow in litres in a set period. We also use a chronometer to calculate the flow rate.

Figure 14 Rate totaliser

Figure 15 Flow path along the flume

3.2.3. Point gauge

The instrument is used to measure vertical distance of the flow or vertical distance of any point within it. The distance is obtained by measuring the depths of two points with an accuracy of one ten thousandth of a meter.

Figure 16 Point gauge

3.2.4. Acoustic Doppler Velocimeter (ADV)

A Nortek AS Vectrino Acoustic Doppler Velocimeter (ADV), was used to measure velocities in the flume. The ADV cylindrical main body is suspended above the flume, with a probe extending into the flow at the end of a thinner cylinder. The transducer in the centre of the probe sends out pairs of brief sound pulses. The sound is subsequently reflected by seeding particles suspended in the water, which have the same mean velocity as the water particles. Four receivers pick up the reflected signal, and the velocity is calculated based on the recorded change in frequency of the sound returned.

Figure 17 Acoustic Doppler Velocimeter

Figure 18 ADV sensors

Note the distribution of the frequency sensors, some sensors are arranged in an oblique downward direction, however, in the ADV used, the almost horizontal orientation of the two lower sensors allows the measurement of velocities at depths closer to the base.

3.2.5. Strain Gauge

Drag forces were recorded with a Cussons Single Component Force Balance shown in Figure 19. A base plate connects four bars that extend downward from the force balance to the top of a cylinder. The top of the force balance is attached to a support structure that sits on a series of rails that run parallel to and above the flume.

The cylinder and the flume base are separated by a short space. The cylinder was hung in the flow for the testing. Because the cylinder height exceeds the allowable depth, the base plate is always elevated over the free surface.

Figure 19 Strain gauge

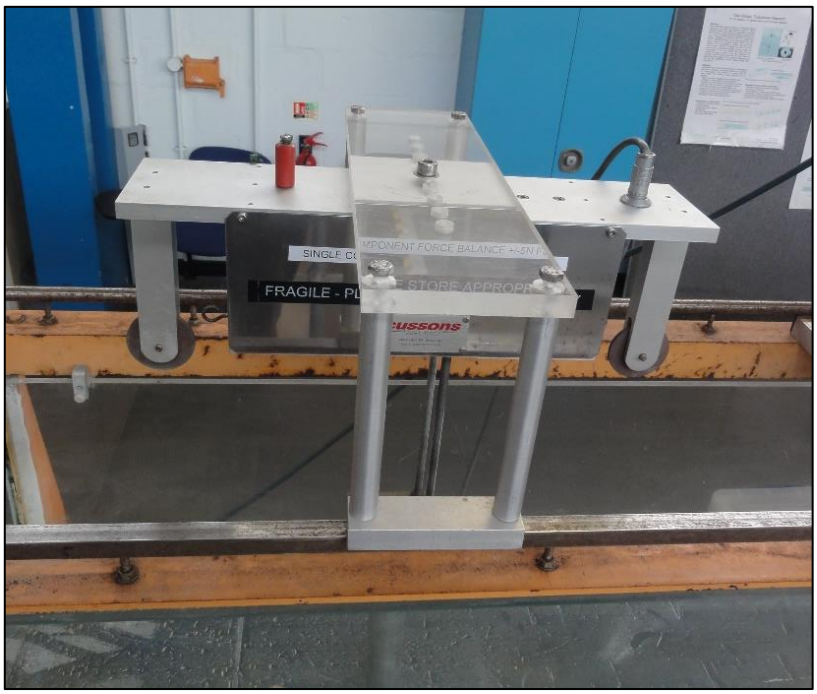

Figure 20 Strain Gauge

The output of the strain gauge is voltage which varies linearly with the deflection. The force acting on the material is a linear function of the output voltage if the material acts linearly and elastically.

3.3. Channel depth

3.3.1. Method

To determine the channel depth, the Point Gauge was used. When the flow is activated in the Flume, it is essential to wait a few minutes until a constant flow is established. When it is visualized that there are no variations in height, the depth of the channel base z1 is read and then the depth of the free surface z2 is taken. The height of the channel is H = z2-z1

3.3.2. Results

	Case 1	Case 2	Case 3
Flow depth (mm)	184.2	181.9	113.7

For the first case, we start the experiments with a depth of 184.2mm, in which the respective flow and velocity will be measured. For the second case, in order to maintain a similar

depth (181.9mm) and increase the speed, we increased the flow, here we observed that the free surface level fluctuated and a totally steady state in the flow was difficult to achieve.

In the third case, in order not to continue increasing the flow, but to continue increasing the speed, the depth was decreased, obtaining 113.7mm.

3.4. Channel velocity profile

3.4.1. Method

Mean velocities were assumed to meet a logarithmic equation for a turbulent boundary layer in the hydraulically smooth regime within the boundary layer near the base of the flume. Outside of the boundary layer, velocities were believed to be uniform and equal to the free-stream value.

The velocity profile was determined in two steps; the first step was to determine the log shape of the boundary layer; the second step was to determine an estimate of the boundary layer depth.

With the data gathered, we are able to determine the typical size of the $v_x(z)$ in relation to the mean velocity.

The Acoustic Doppler Velocimeter (ADV) was used to measure mean velocities at eleven points in space. Vertical velocity profiles were measured at the centre of the length and along the channel centreline.

3.4.2. Results

Table 3 shows the average velocities in X direction (along the flume depth) collected by the ADV for each height measured from the base of the channel.

Figure 21 shows the ADV output at a height measured from the bottom of the channel z=10mm, while Figure 22 shows the output at z=155mm. For a better visualization, a range of 30 seconds is shown, from t = 30s to t = 60s.

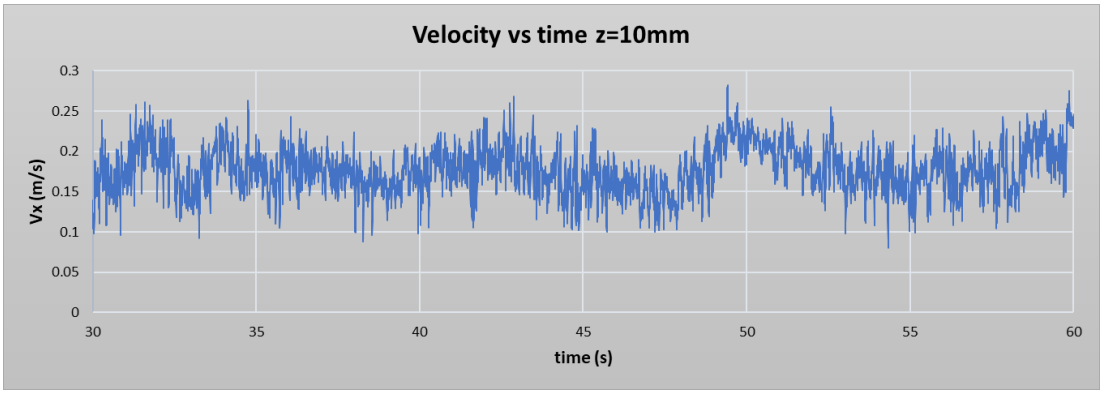

Figure 21 Velocity measured by ADV at z=10mm

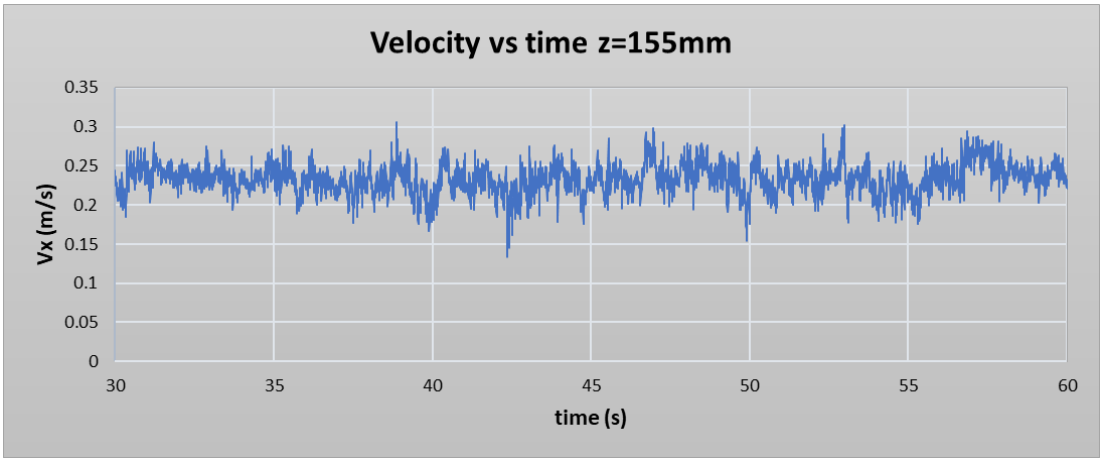

Figure 22 Velocity measured by ADV at z=155mm

First we can see a greater variability in the measurements at z=10mm, compared to those at z=155mm. In the next section we will see in more detail the variation of both the mean velocity and the standard deviation along the height of the channel.

In Table 3 it is summarized the mean velocities at each of the eleven points measured. As well as it is plotted in Figure 23 and Figure 24. These graphs clearly show the shape of the described velocity profile described in 2.2.2.

Flow depth $H = 177.2mm$

Table 3 Velocity profile values in X direction

Point	Z(mm)	$v_x(z)$ (m/s)	z/H	v/V_m
1	10	0.184	0.056	0.841
2	14	0.206	0.079	0.941
3	24	0.219	0.135	1.001
4	35	0.221	0.198	1.009
5	44	0.229	0.248	1.048
6	58	0.230	0.327	1.051
7	79	0.231	0.446	1.056
8	97	0.231	0.547	1.054
9	117	0.231	0.660	1.053
10	142	0.231	0.801	1.054
11	155	0.233	0.875	1.065

Mean velocity Vm = 0.219 m/s

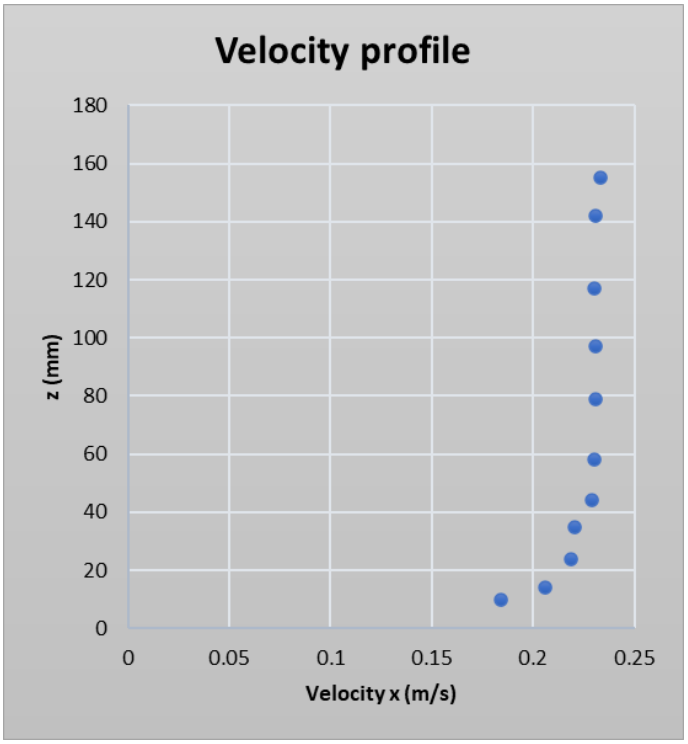

Figure 23 Velocity profile m/s

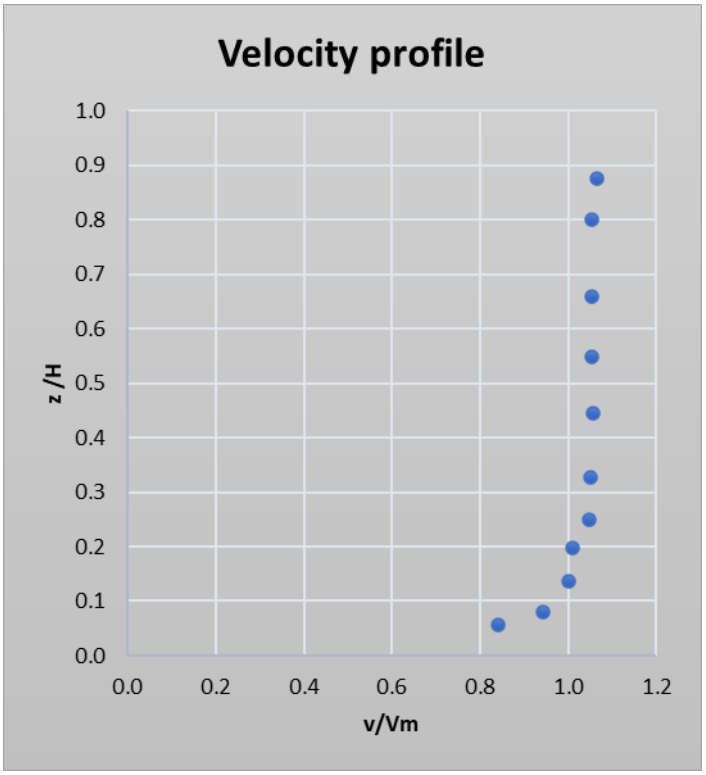

Figure 24 Velocity profile V/Vm

From the data collected and shown in the graph, we can obtain the height of the boundary layer δ, that is $0.3H$, the velocity from this height remains consistently uniform.

Secondary Components

In the same way, the velocity components in the Y and Z directions were obtained, and they are shown in Table 4 and Table 5.

Table 4 Velocity profile values in Y direction

Point	z(mm)	v_y(z) m/s
1	10	0.022
2	14	0.026
3	24	0.029
4	35	0.022
5	44	0.022
6	58	0.02
7	79	0.004
8	97	-0.011
9	117	-0.017
10	142	-0.009
11	155	-0.009

Table 5 Velocity profile values in Z direction

Point	z(mm)	v_z(z) m/s
1	10	0.002
2	14	0.006
3	24	0.010
4	35	0.014
5	44	0.020
6	58	0.022
7	79	0.023
8	97	0.022
9	117	0.018
10	142	0.007
11	155	0.004

Figure 25 and Figure 26 show the average velocities in the Y and Z direction respectively, which have particular shapes and are similar to previous works done by other authors.

It is especially interesting to observe that the velocity component in Y turns to the opposite direction right in the middle of the channel height. Moreover, in the Z direction, the velocity component reaches its highest value in the middle of the channel height, and it is practically zero at the bottom and at the top of the channel.

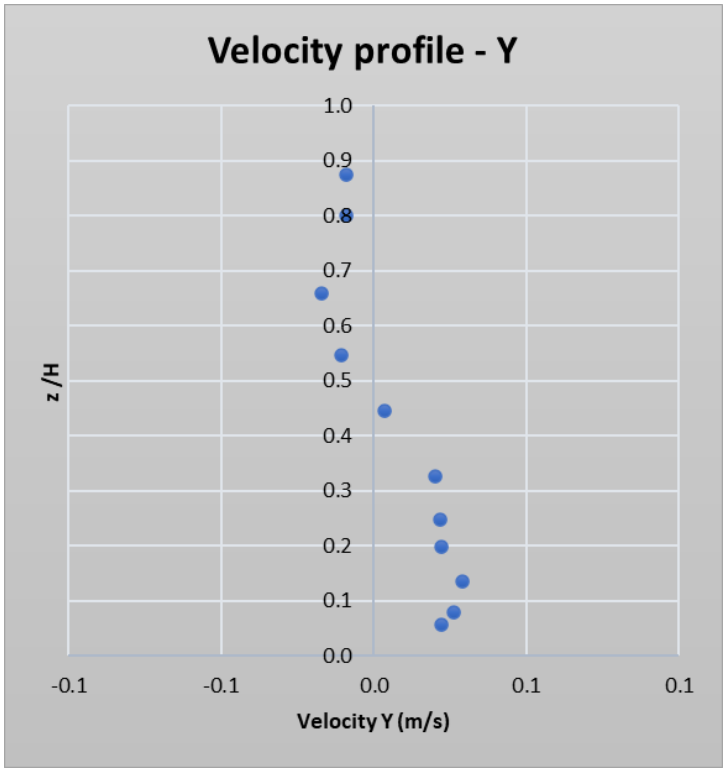

Figure 25 Velocity profile in Y direction (m/s)

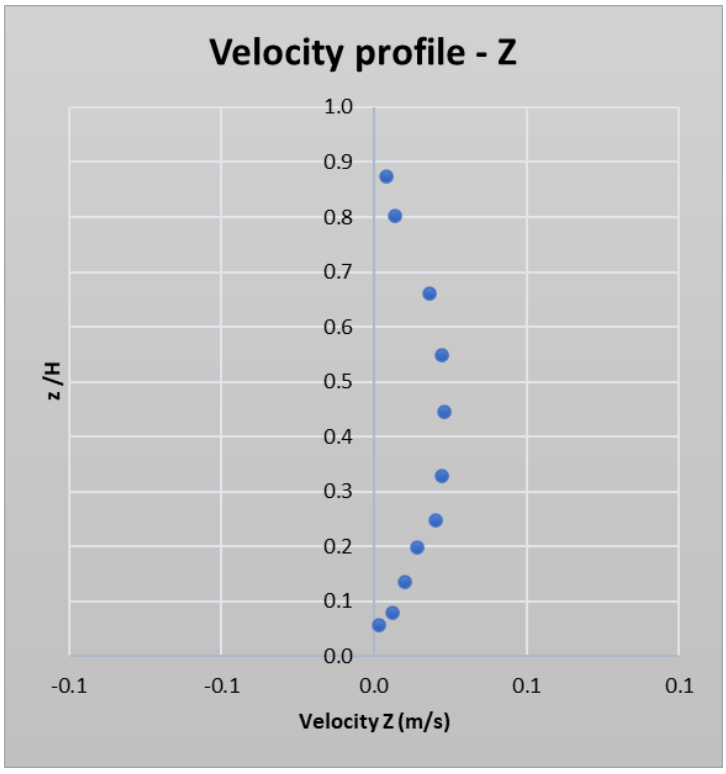

Figure 26 Velocity profile in Z direction (m/s)

Shown velocity values are relatively small; in the Y direction, the maximum velocity represents 12% of the velocity in the main flow direction X, while the velocity in the Z direction is about 10%, then they can be neglected in our analysis.

Standard Deviation

The standard deviation is an indicator of the level of turbulence that occurs in the channel. Table 6 shows the standard deviation values for each direction and the resultant calculated as follow:

$$\sigma = \sqrt{{\sigma_x}^2 + {\sigma_y}^2 + {\sigma_z}^2}$$

Table 6 Standard deviation - three directions and resultant

Point	z(mm)	σx (m/s)	σy(m/s)	σz(m/s)	σ(m/s)
1	10	0.030	0.023	0.032	0.050
2	14	0.029	0.024	0.027	0.046
3	24	0.026	0.022	0.025	0.042
4	35	0.024	0.023	0.025	0.041
5	44	0.021	0.021	0.024	0.038
6	58	0.022	0.023	0.026	0.041
7	79	0.023	0.022	0.028	0.042
8	97	0.022	0.019	0.030	0.041
9	117	0.020	0.018	0.026	0.038
10	142	0.018	0.018	0.023	0.034
11	155	0.019	0.019	0.023	0.035

The maximum value of σ is at the level closest to the surface, with a value of 0.05 m/s Figure 27 shows the turbulence intensity along the height of the channel over a period of 60s.

Table 7 Turbulence intensity along the height

z/H	TI %
0.06	27.1%
0.08	22.3%
0.14	19.3%
0.20	18.6%
0.25	16.6%
0.33	17.8%
0.45	18.3%
0.55	17.9%
0.66	16.5%
0.80	14.7%
0.87	15.2%

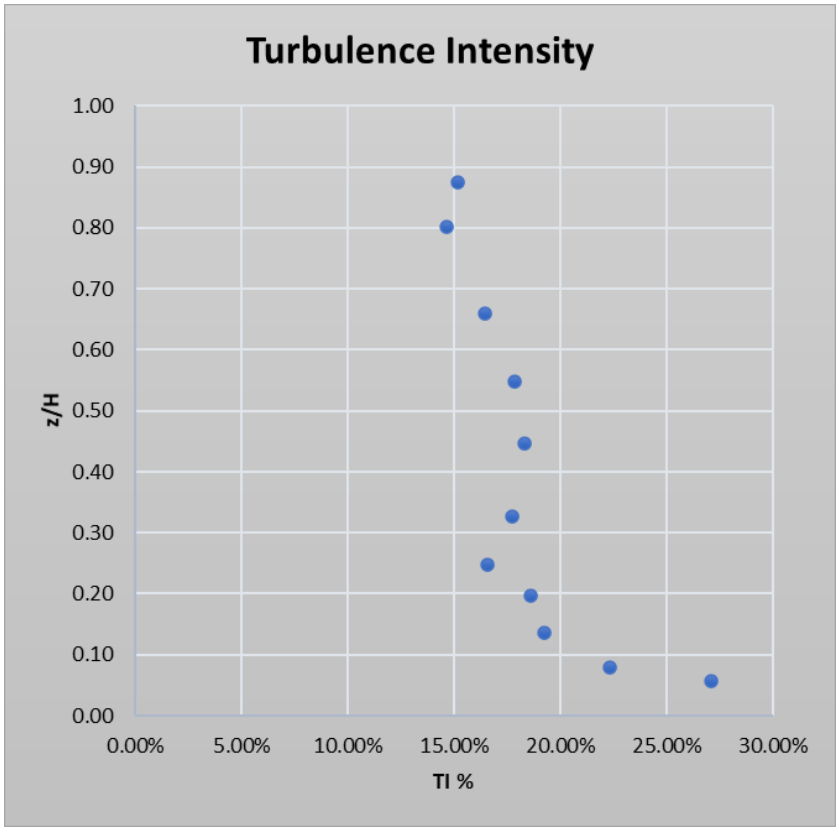

Figure 27 Turbulence Intensity profile

The unobstructed channel has an average turbulence intensity of about 17%, with a visible increase in the bottom of the channel where it reaches 27%.

3.5. Flow Rate and Mean Velocity

3.5.1. Method

The flow rate is calculated from two values that we can measure during the experiments, the volume of water that flows and the time it takes for this volume to flow.

$$Q = \frac{Vol}{t}$$

The mean velocity is calculated by the ratio of the flow rate and the area of the cross-section flow.

$$V_m = \frac{Q}{A}$$

$$A = B.H$$

Where the channer width B is constant B=0.3m

3.5.2. Results

Table 8 Rate flow and mean velocity for cases 1, 2 and 3

	Case 1	Case 2	Case 3
Rate Flow (m3/s)	0.012	0.019	0.015
Mean Velocity (m/s)	0.213	0.354	0.426

3.6. Obstacles

Figure 28 and Figure 29 shows the tubes used for the analysis of drag forces. In this study, the geometry of the obstacles varies in order to obtain different degrees of flexibility, while keeping the same modulus of elasticity. The three tubes have the same diameter but different wall thicknesses. The mechanical properties are shown below:

Figure 28 tubes

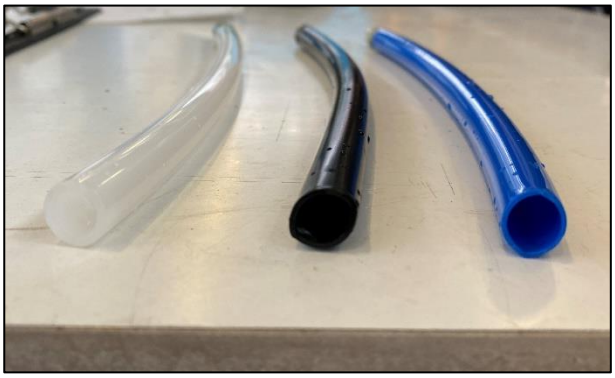

Figure 29 tubes – sections

Obstacles Geometry

- Cylinder 1 - *White*

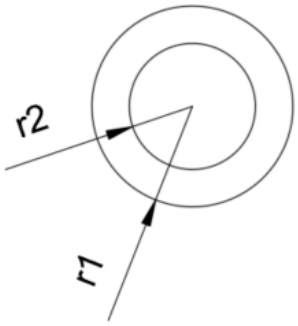

Radius 1	r1	6	mm
Radius 2	r2	5	mm
Thickness	t1	2	mm
Height	h_0	250	mm

- Cylinder 2 – Black

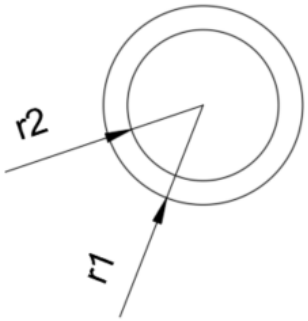

Radius 1	r1	6	mm
Radius 2	r2	4.5	mm
Thickness	t2	1.5	mm
Height	h_0	250	mm

- Cylinder 3 - Blue

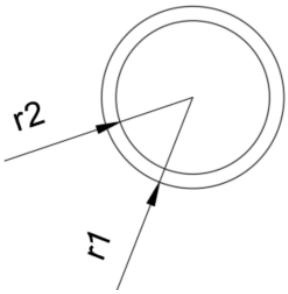

Radius 1	r1	6	mm
Radius 2	r2	4	mm
Thickness	t3	1	mm
Height	h_0	250	mm

Obstacles Mechanical Properties

The tree cylinders are made with polyamide 12, this flexible material has a range of modulus of elasticity of 1.70 $x10^9$ – 1.90 $x10^9$ N/mm2, for the purpose of this study, we consider 1.8$x10^9$ N/mm2.

- Cylinder 1 – White t2

Modulus of Elasticity	E	1.80E+09	N/mm2
Thickness	t_1	2	mm
Area	A_1	0.0001	m2
Second moment Area	Iy_1	8.17E-10	m4
Slenderness	S_R	83.33	

- Cylinder 2 – Black t1.5

Modulus of Elasticity	E	1.80E+09	N/mm2
Thickness	t_2	1.5	mm
Area	A_2	0.0000	m2
Second moment Area	Iy_2	6.96E-10	m4
Slenderness	S_R	83.33	

- Cylinder 3 – Blue t1

Elasticity Modulus	E	1.80E+09	N/mm2
Thickness	t3	1	mm
Area	A_3	3.46E-05	m2
Second moment Area	Iy_3	5.27E-10	m4
Slenderness	S_R	83.33	

The elements are placed at the longitudinal and transverse centre of the flume, as shown in the sketches of Figure 30 and Figure 31.

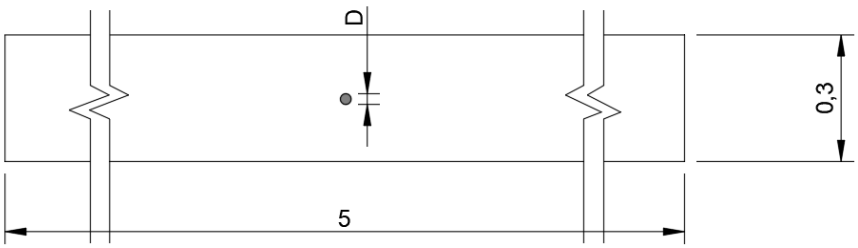

Figure 30 Plane view of single cylinder

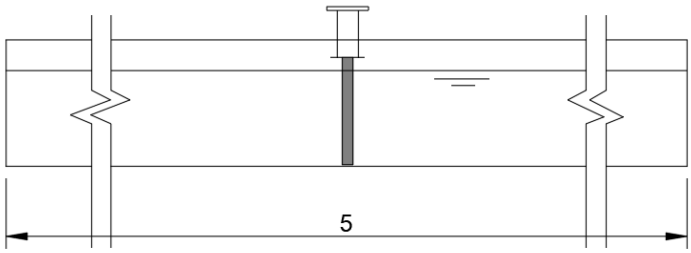

Figure 31 Elevation of single cylinder

4. ISOLATED FLEXIBLE CYLINDERS

4.1. Forces on the Cylinders

4.1.1. Aim

The objective of the laboratory experiments is to obtain the drag forces on three types of flexible obstacles in three types of flows and to determine the drag coefficient of the same. The determined values will be compared with those obtained by other authors, in order to find similarities, variations, and ranges of coincident parameters.

In addition, we will determine the relationship between the drag coefficients of flexible obstacles with those found in previous research for rigid obstacles of the same characteristics.

Furthermore, we will also discuss the relationship of drag coefficients with the Reynolds number and with the stiffness of the obstacles.

4.1.2. Method

Calibration

Strain gauge calibration is performed by measuring previously known masses. The data obtained gives us the relationship between the forces and the voltage of the equipment. For this test we use masses of 100g, 200g and 300g first on the left-hand side, and then on the right-hand side. A schematic calibration in one side is shown in Figure 32.

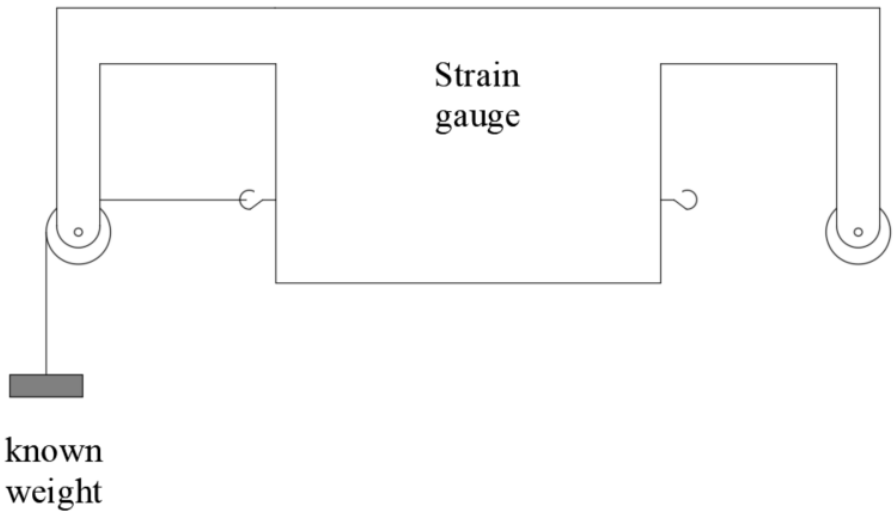

Figure 32 Force balance sketch - One side

Voltage equivalence

Left hand side

mass 1	m1	-100	g
mass 2	m2	-200	g
mass 3	m3	-300	g

Right hand side

mass 1	m1	100	g
mass 2	m2	200	g
mass 3	m3	300	g

Forces in cylinders

Figure 33 shows the sketch of the force measurement in the cylinders. Three separate sets of measurements were taken, each one with the characteristics described in the previous chapter. For all of them, the slope considered is zero.

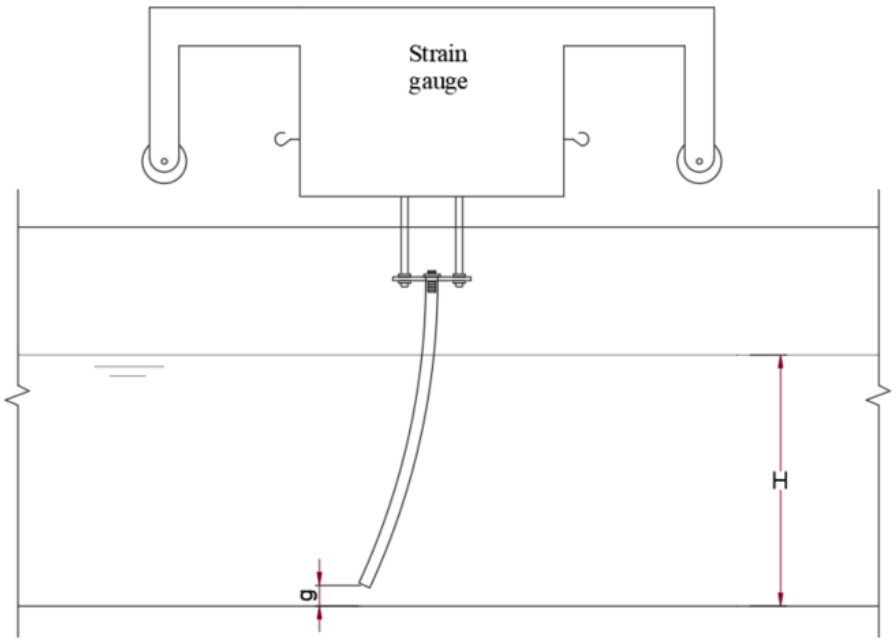

Figure 33 Force measurement sketch

The cylinders were bolted to the metal plate of the strain gauge. The cylinders were suspended in the channel, we can see a small gap between the cylinder and the base of the channel, which we call "g". When the flow is established, we proceed to record the voltage; the drag force considered will be the average of the forces recorded over 60 seconds.

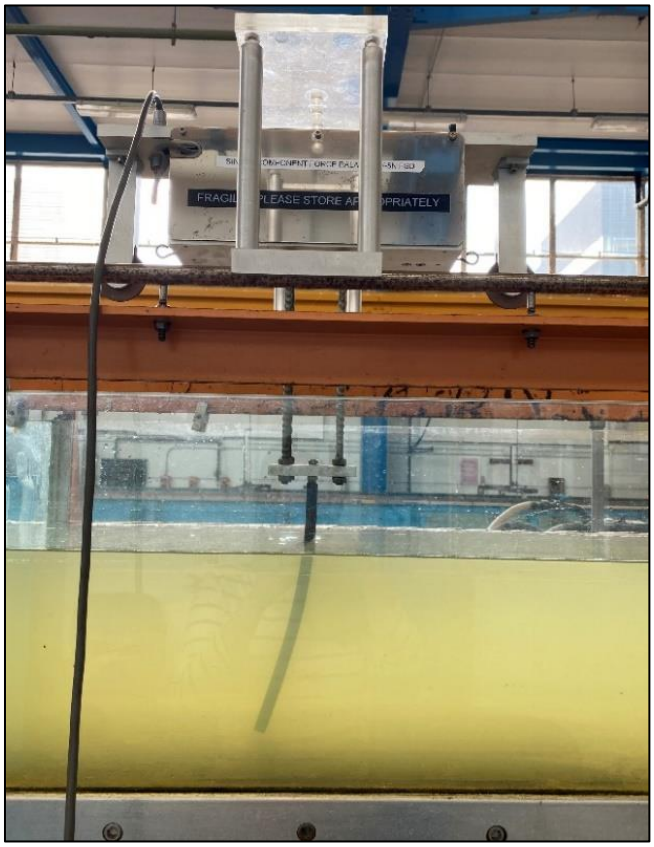

Figure 34 Force measuring - Case 1

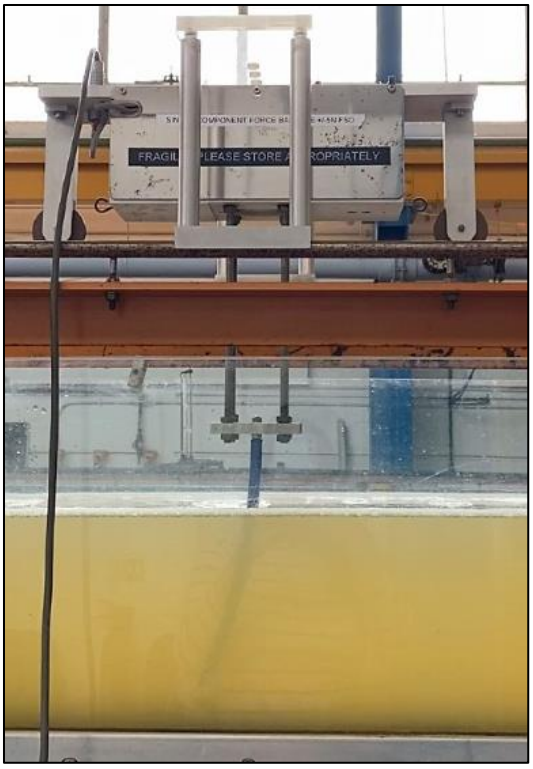

Figure 35 Force measuring - Case 2

Figure 36 Force measuring - Case 3

4.1.3. Results

Calibration

Figure 37 shows the measurements in volts taken for 60 seconds at each of the 3 forces applied to both sides of the strain gauge.

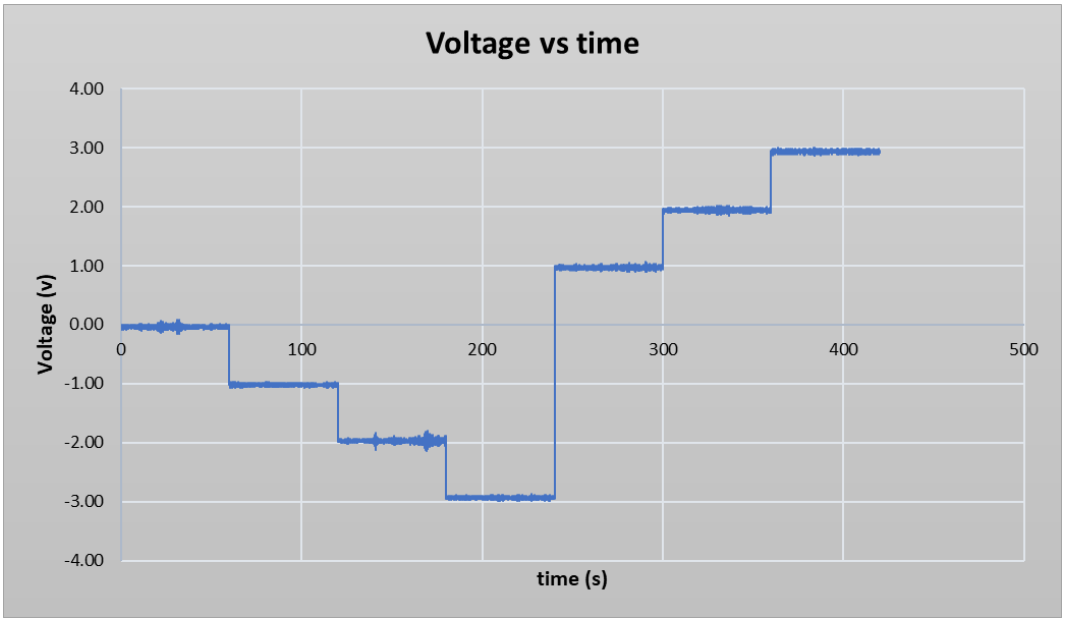

Figure 37 voltage vs time

With the data collected, we proceed to plot the graph that shows the relationship between the voltage read and the applied force.

Left hand side

mass 1	m1	-100	g	-0.981	N	-0.134	V
mass 2	m2	-200	g	-1.962	N	-0.249	V
mass 3	m3	-300	g	-2.943	N	-0.365	V

Right hand side

mass 1	m1	100	g	0.981	N	0.108	V
mass 2	m2	200	g	1.962	N	0.225	V
mass 3	m3	300	g	2.943	N	0.346	V

Then, the graph force vs voltage is as follows:

Table 9 Voltage output and force equivalent

Voltage (V)	Force (N)
-0.37	-2.943
-0.25	-1.962
-0.13	-0.981
0.11	0.981
0.23	1.962
0.35	2.943

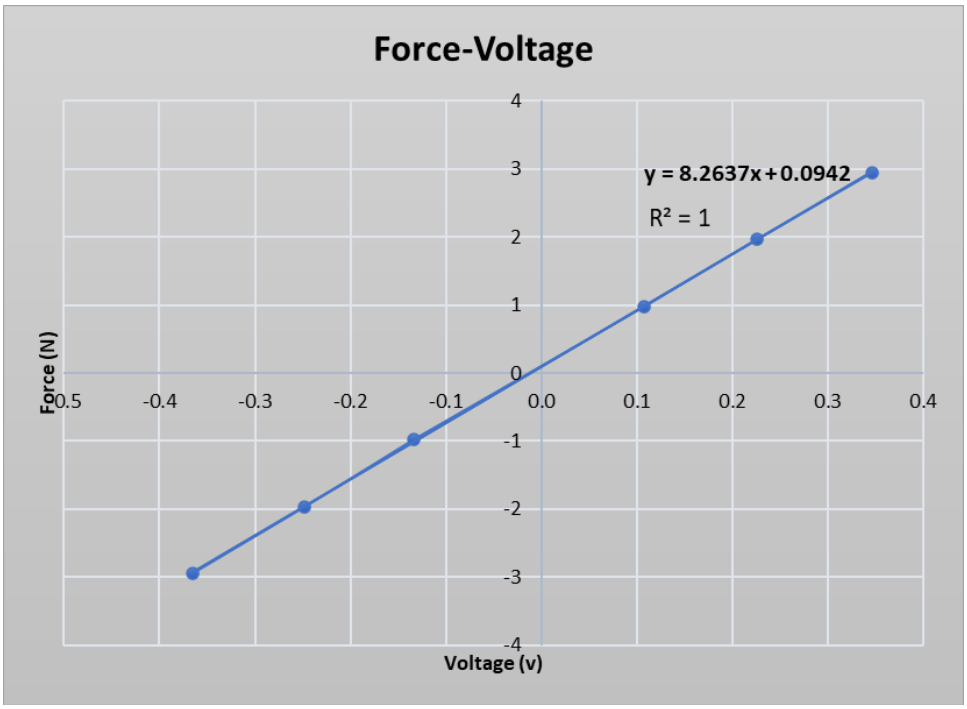

Figure 38 Force – voltage

$$F = 8.264(V_{out}) + 0.094 \tag{40}$$

where V_{out} is the average voltage in volts and F is the applied force in Newtons.

Equation (40) may be used to determine the drag force when the force balance is aligned with the mean flow direction. The R^2 value is more than 0.99, suggesting that the expression is very accurate for the measured data.

Forces on the cylinders

Figure 39 shows the obstacles during the experiments for the three cases. It is clear the different flow path generated in each case. In the first case we can see a few weak vortices, while in case 2 and 3 the vortices are more visible; and in the case 3, the boundary layer is more separated than in case 2.

Figure 39 Experiment case 1 Re=2736 / Experiment case 2 Re=4260 / Experiment case 3 Re=5508

The different load paths affect the drag forces measured. One of the indicators of this effect is the standard deviation, which we will be able to discuss for each case when we analyse it in the following sections.

To illustrate the output from the strain gauge, Figure 40 and Figure 41 shows the forces measured in a range of 10 seconds from t=40s to t=50s, for the case 1 and case 3 respectively, on the obstacle 1 - White.

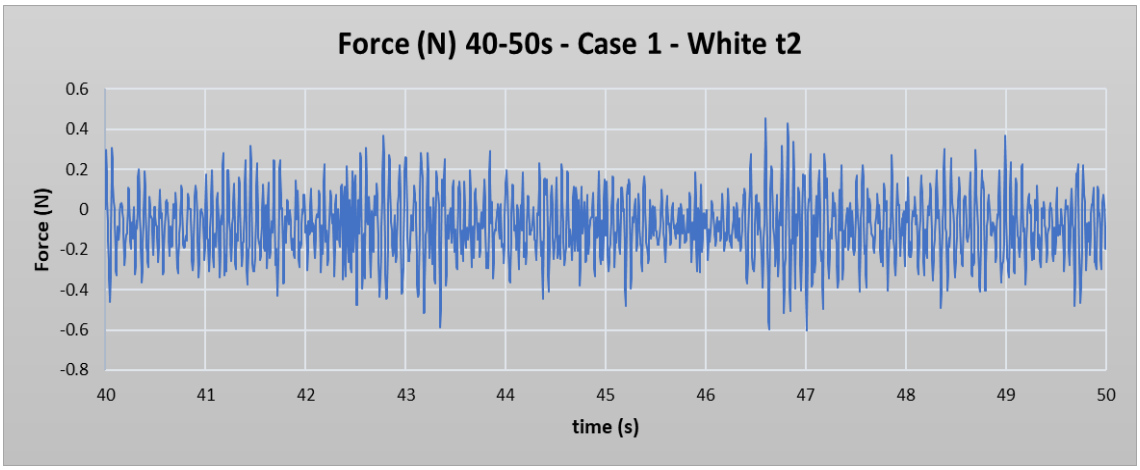

Figure 40 Force measured in the case 1 on the Obstacle 1 White

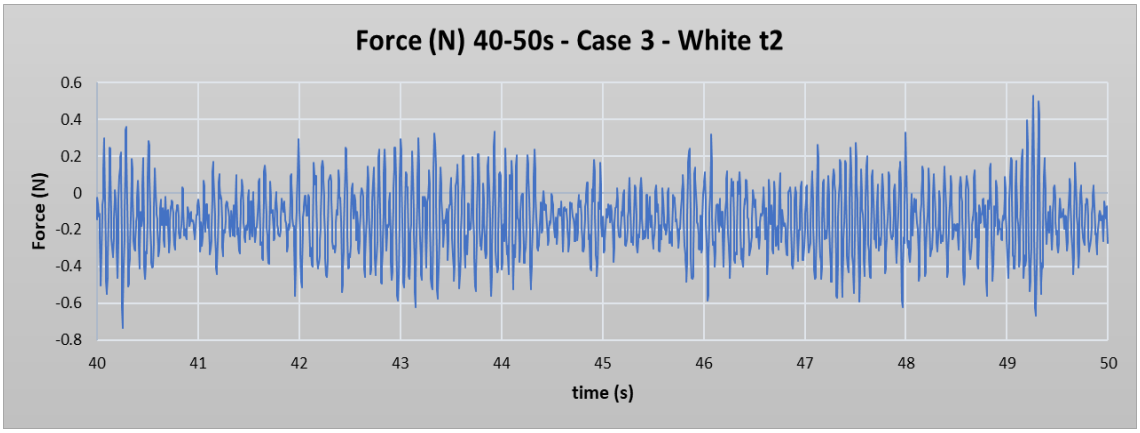

Figure 41 Force measured in the case 3 on the Obstacle 1 White

From the graphs, we can preliminarily observe a high dispersion, and detect figures of up to six times the average force. In more detail, we can observe forces obtained on the three types of obstacles for the three cases studied in the following summary.

- *Case 1*

Mean velocity	Vm	0.228	m/s
Reynolds number	Re	2736	

		Obstacle 1 - White	Obstacle 2 - Black	Obstacle 3 - Blue
Average force	FD (N)	-0.086	-0.084	-0.086
Maximum force	FD max (N)	0.658	0.604	0.666
Minimum force	FD min (N)	-0.709	-0.886	-0.811

- *Case 2*

Mean velocity	Vm	0.355	m/s
Reynolds number	Re	4260	

		Obstacle 1 - White	Obstacle 2 - Black	Obstacle 3 - Blue
Average force	FD (N)	-0.164	-0.166	-0.166
Maximum force	FD max (N)	0.628	0.693	0.693
Minimum force	FD min (N)	-0.943	-1.002	-1.029

- *Case 3*

Mean velocity	Vm	0.459	m/s
Reynolds number	Re	5508	

		Obstacle 1 - White	Obstacle 2 - Black	Obstacle 3 - Blue
Average force	FD (N)	-0.153	-0.147	-0.150
Maximum force	FD max (N)	0.598	0.668	0.544
Minimum force	FD min (N)	-0.862	-0.881	-0.870

The Reynolds number of each case can be used to characterise the range of experimental circumstances for uniform flow, in this case based on cylinder diameter. For this study, all

the Re are less than 10^5, and they will be used to determine whether the drag coefficient is a function of Re within this range.

- *Standard deviation*

Table 10 Force Standard deviation for the three type of obstacles

	Vm (m/s)	σ (N)
White t2	0.228	0.177
White t2	0.355	0.187
White t2	0.459	0.189
Black t1.5	0.228	0.190
Black t1.5	0.355	0.194
Black t1.5	0.459	0.200
Blue t1	0.228	0.180
Blue t1	0.355	0.186
Blue t1	0.459	0.195

The standard deviation shows high-level values, that reach 100% to 200% of the average total force, this shows that the obstacle is subjected to a high vibration within the flow. We will determine in the next chapter whether it is related to the velocity of the flow.

4.2. Deformation of the Cylinders

4.2.1. Aim

The main aim of this stage is to verify the mechanical behaviour of the obstacle through the finite element analysis in the software Ansys 2019 R3 of the element subjected to the forces find in the experimental process.

4.2.2. Method

The analysis method used will be Linear Elastic. This analysis should assume that the stress-strain behaviour of the material is linear. Additionally, internal forces may be calculated according to elastic global analysis. The model considered is a 3D body subjected to a distributed load and fixed in the bottom end.

Idealization of the element

In this study, a simple cantilever member is exposed to horizontal loads. The height of the member is 0.25 m long. The following figure shows an actual example, geometry, dimensions, and boundary conditions of the member to be analysed.

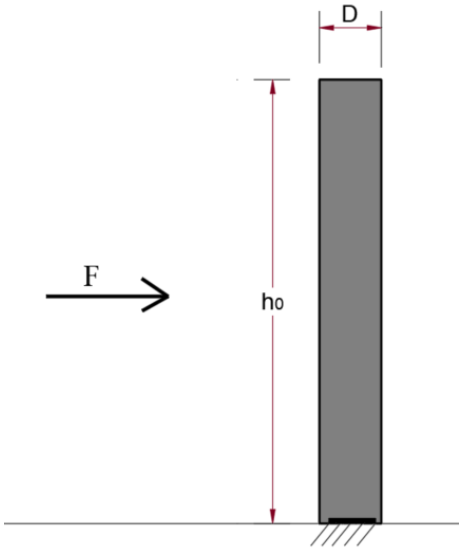

Figure 42 Idealization of the problem

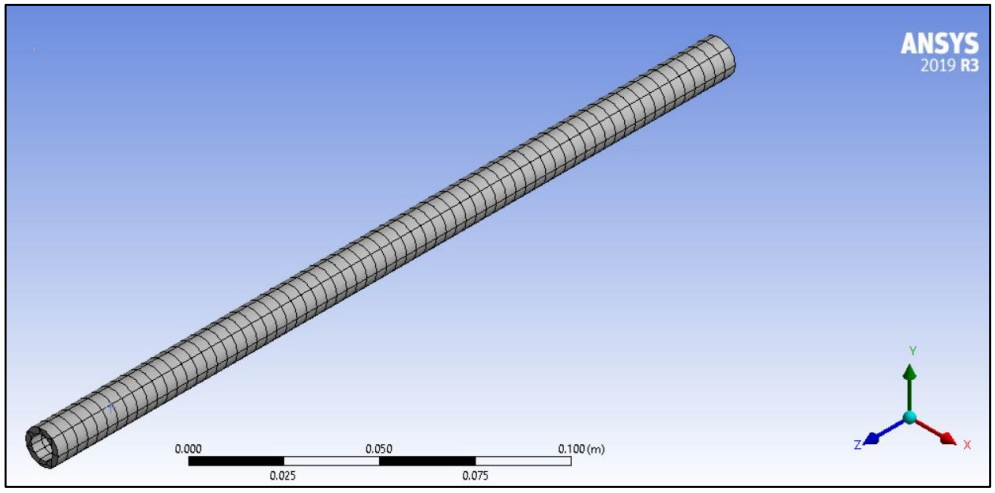

Figure 43 cylinder model

Boundary conditions

- Constrains:

  In Figure 44 it is shown that the constrains are assigned to joints in the bottom end, the joints are restricted in displacement and rotation in the three directions.

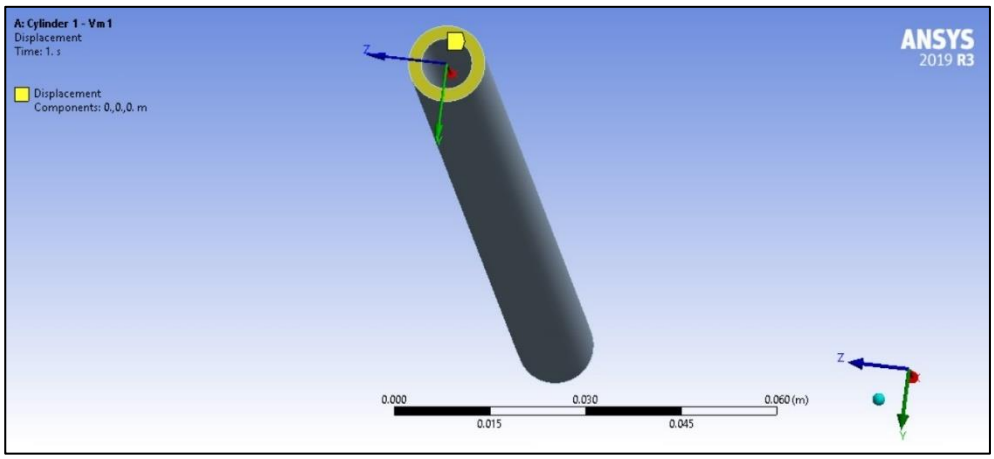

Figure 44 cylinder model - constrains

- Loads:

  For convenience, the total drag force F_D will be applied to the model as pressure on the cylinder in one of the directions perpendicular to its length, in this case the Z direction.

  The applied pressure results from dividing the force F_D by the surface area of the cylinder within the flow, which is, the perimeter of the cross-section times the flow depth.

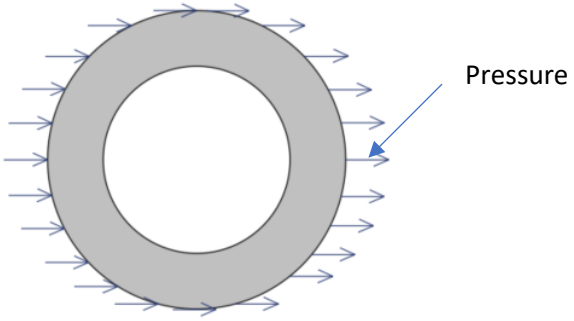

Figure 45 pressure distribution in cross-section

For the Obstacle White, t=2mm

	F_D (N)	H (m)	Surface (m^2)	Pressure (Pa)
Case 1	0.0864	0.184	0.007	12.44
Case 2	0.1643	0.182	0.007	23.96
Case 3	0.1528	0.114	0.004	35.65

For the Obstacle Black, t=1.5mm

	F_D (N)	H (m)	Surface (m^2)	Pressure (Pa)
Case 1	0.0841	0.184	0.007	12.11
Case 2	0.1663	0.182	0.007	24.25
Case 3	0.1472	0.114	0.004	34.35

For the Obstacle Blue, t=1mm

	F_D (N)	H (m)	Surface (m^2)	Pressure (Pa)
Case 1	0.0864	0.184	0.007	12.44
Case 2	0.1643	0.182	0.007	23.96
Case 3	0.1528	0.114	0.004	35.65

4.2.3. Results

Figure 46 a, b, shows the program results of the deformations of the element, in this case for the obstacle 1 white.

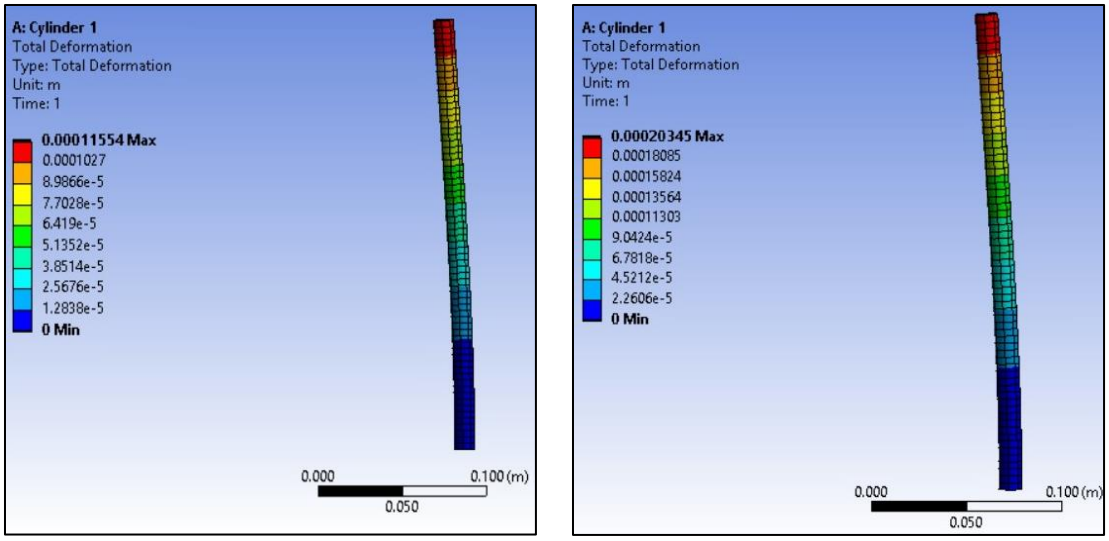

Figure 46 cylinder deformation

Table 11 summarizes the maximum displacements obtained for the 3 cylinders in the 3 cases tested.

Table 11 Maximum deformation of cylinders

	Maximum deformation (mm)		
	cylinder 1	cylinder 2	cylinder 3
Case 1	0.11	0.12	0.19
Case 2	0.18	0.24	0.36
Case 3	0.20	0.28	0.43

As expected, the deformations increase the more flexible the cylinder and the higher the flow velocity. These values will be used to determine the area of the section exposed to the flow in each condition.

5. DISCUSSION

5.1. Drag Forces

5.1.1. Relationship of Drag force with Velocity

Because in each case studied the flow depths are different, we divide the total drag forces obtained by the projected area in the direction of the flow Ap. This allows us to study the relationship of force and velocity. We call this force per unit area f_D, shown in Figure 47 as a function of the velocity Vm.

$$f_D = \frac{F_D}{A_p}$$

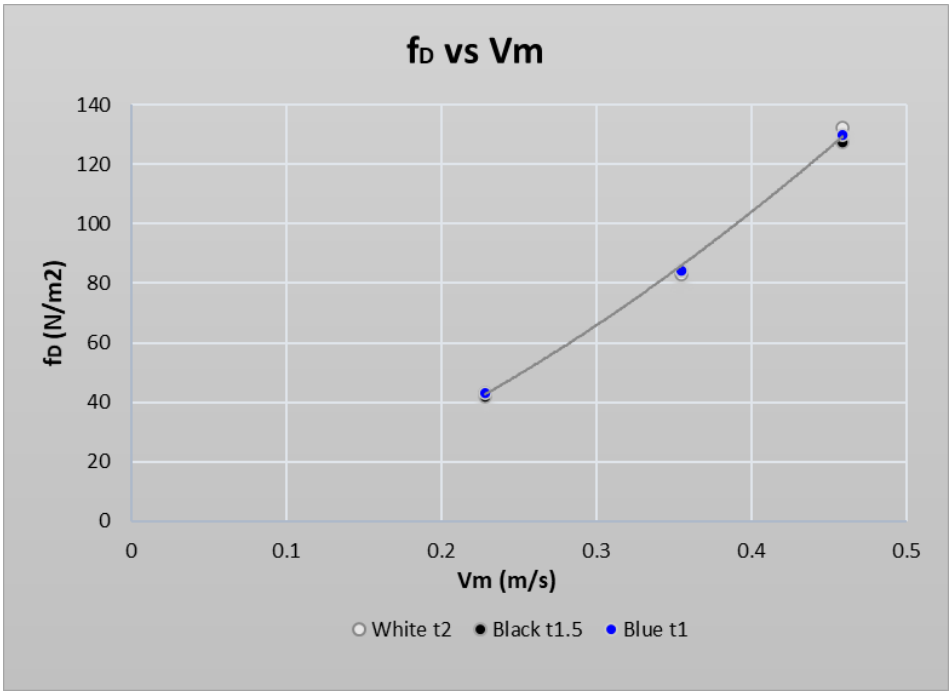

Figure 47 Force per unit area vs Velocity

$$f_D \propto V^{1.6}$$

For rigid elements, the drag force is a quadratic function of the velocity. For flexible elements, as a result of static and dynamic reconfiguration, the relationship varies as identified by Vogel, and as mentioned in the section 2.3.4. Vogel number ψ is a measure of deviation from expected behaviour for rigid bodies. For a flexible element, one can expect $\psi < 0$ (Albayrak, Nikora, Miler, & O'Hare, 2011).

For this study, we get indeed $\psi = -0.4 < 0$

5.1.2. Standard Deviation

Figure 48 shows the standard deviation in relation to the Reynolds number for the three types of obstacles.

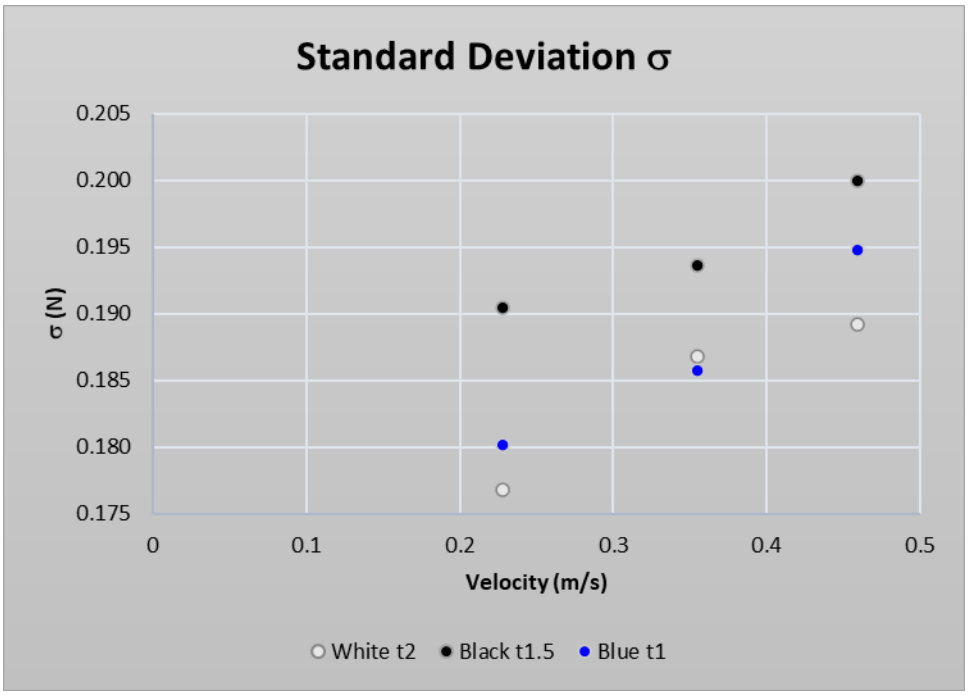

Figure 48 Standard deviation vs Velocity

The σ is strongly affected by the velocity for all stiffnesses. It can be seen from the graph that σ is greater when the velocity increases.

5.2. Drag Coefficient

5.2.1. Drag Coefficient calculated from the experiments

Both Model 1 (Chapman, Wilson, & Gulliver, 2015) and Model 2 (Whittaker, Wilson, & Aberle, 2015) were used to calculate the drag coefficients for the elements tested, results are shown in Table 12 and Table 13.

Table 12 Drag coefficient - Model 1

	Vm (m/s)	β	H (m)	Re	Ca	F (N)	CD
White t2	0.228	0.999	0.184	2736	1.04E-04	0.086	1.67
White t2	0.355	0.998	0.182	4260	2.43E-04	0.164	1.33
White t2	0.459	0.996	0.114	5508	9.93E-05	0.153	1.26
Black t1.5	0.228	0.999	0.184	2736	1.04E-04	0.084	1.62
Black t1.5	0.355	0.998	0.182	4260	2.43E-04	0.166	1.34
Black t1.5	0.459	0.995	0.114	5508	9.93E-05	0.147	1.22
Blue t1	0.228	0.998	0.184	2736	1.04E-04	0.086	1.67
Blue t1	0.355	0.998	0.182	4260	2.43E-04	0.166	1.34
Blue t1	0.459	0.994	0.114	5508	9.93E-05	0.150	1.24

Table 13 Drag coefficient - Model 2

	Vm (m/s)	H (m)	Re	Ca	F (N)	CD
White t2	0.228	0.184	2736	2.40E-03	0.086	1.66
White t2	0.355	0.182	4260	5.60E-03	0.164	1.32
White t2	0.459	0.114	5508	2.14E-03	0.153	1.26
Black t1.5	0.228	0.184	2736	2.82E-03	0.084	1.62
Black t1.5	0.355	0.182	4260	6.57E-03	0.166	1.34
Black t1.5	0.459	0.114	5508	2.52E-03	0.147	1.21
Blue t1	0.228	0.1842	2736	3.72E-03	0.086	1.66
Blue t1	0.355	0.1819	4260	8.67E-03	0.166	1.34
Blue t1	0.459	0.1137	5508	3.32E-03	0.150	1.24

Although both models consider and incorporate their own parameters, as well as they have some variations in the calculation of the drag coefficient, the computed C_D are mainly similar; therefore, for our Re range, we could use either Model 1 or 2. This similarity is more appreciable in Figure 52, where C_D from both model are plotted.

5.2.2. Drag Coefficient from previous works

White 1991

In the textbook we find the following relationship between the drag coefficient and Re. (White, 1991).

Drag coefficient vs Re, Re<10^5.

$$CD = 1 + 10.0Re^{-2/3} \tag{41}$$

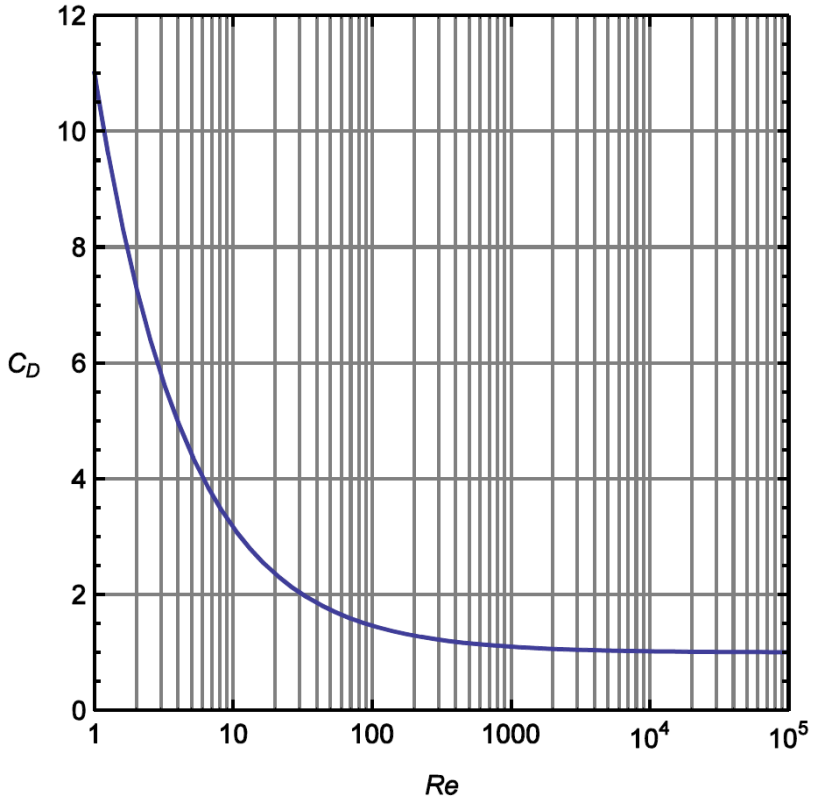

Figure 49 Relation of CD and Re (White, 1991)

Later studies demonstrated that the expression would underestimate CD for low Reynolds numbers and overestimate CD for high Reynolds numbers. Therefore, we will see in the next item that it is possible to adjust this relationship.

Chang & Nguyen:

In order to compare the drag coefficients obtained in this study with those obtained for rigid elements, we chose the results obtained by Chang & Nguyen (2011). The researchers did multiple experiments with emergent vegetation, and made a compilation work from different authors, where they obtained the following graph and formula that relates C_D and Re based on the hydraulic radius.

Drag coefficient vs Re, $Re<10^6$.

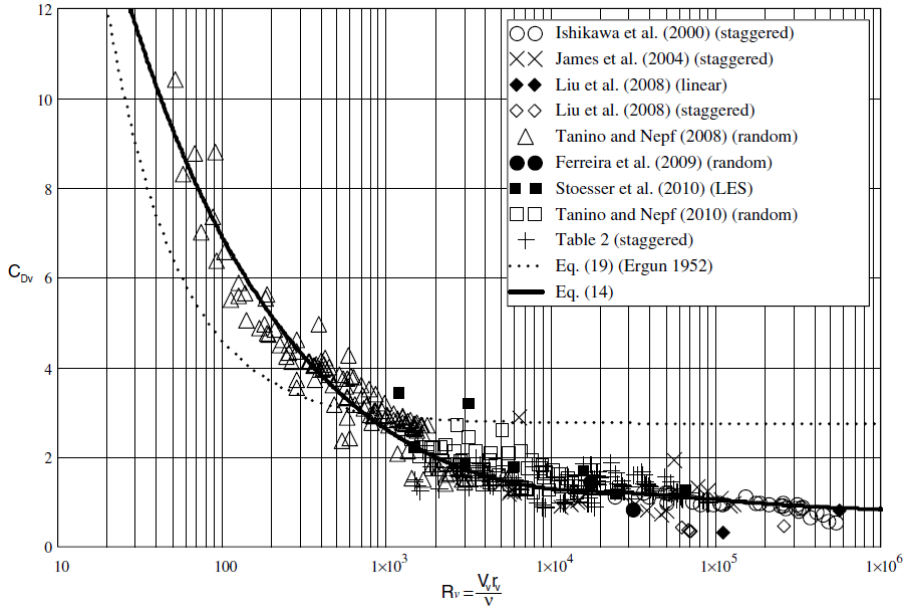

Figure 50 Drag Coefficient vs Re (Cheng & Nguyen, 2011)

$$CD = \frac{50}{Re^{0.43}} + 0.7[1 - \exp\left(-\frac{Re}{15000}\right)] \quad (42)$$

In the following sections we will consider the statements given by Cheng and Nguyen for rigid elements, in order to compare the coefficients obtained in this experimental work with flexible objects under the same flow characteristics.

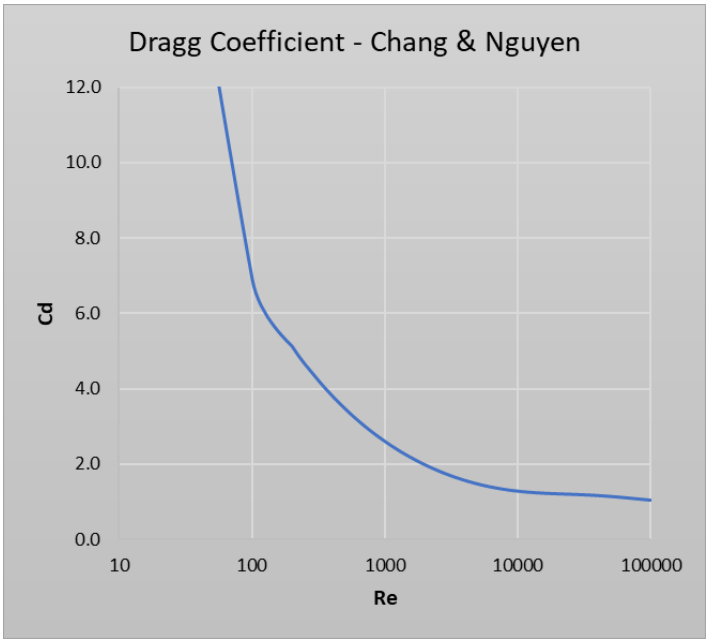

Figure 51 Cd as a function of Re according to CHANG & NGUYEN

5.3. Variation in function of the Velocity and Reynolds number

Drag Coefficient vs Reynolds Number

Figure 52 shows the C_D drag coefficients obtained with both models vs. Reynolds number based on cylinder diameter. For the range of Re in which the tests in this dissertation are found, the equation that describes the curve is a logarithmic function, as seen below.

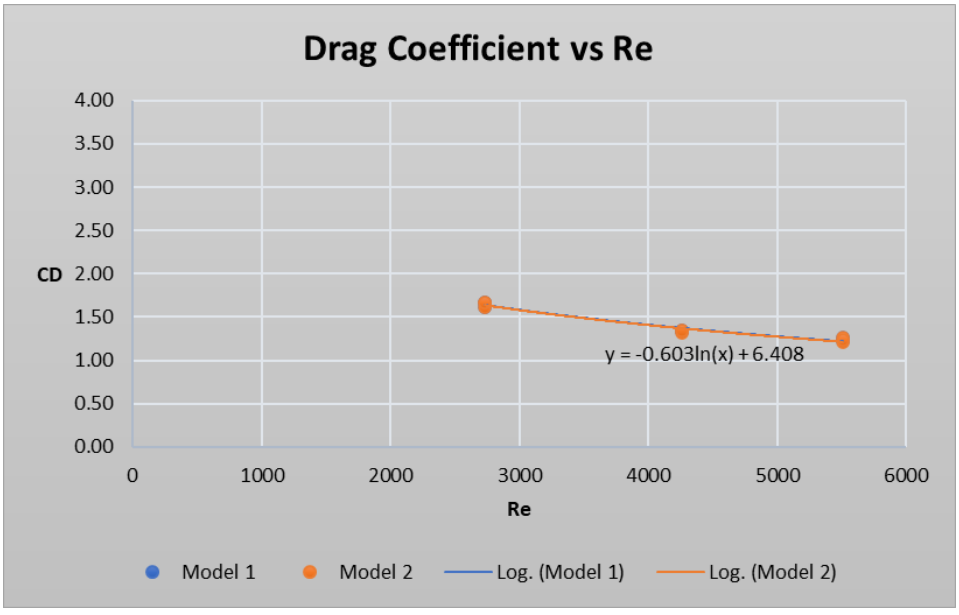

Figure 52 Drag coefficient vs Re

For the range of Re of this study, we have:

$$C_D = -0.65 \ln(Re) + 6.99 \tag{43}$$

It is appreciated that the logarithmic expression in Equation (43) is highly similar to that obtained by Chapman, Wilson, & Gulliver (2015) shown in equation (44) and plotted in Figure 53. It is important to mention that this author's tests were performed for lower values of Re.

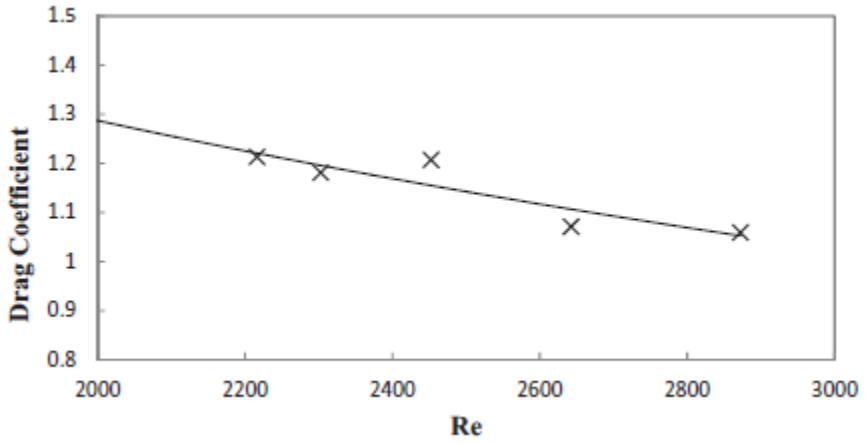

Figure 53 Drag coefficient vs Re (Chapman, Wilson, & Gulliver, 2015)

$$C_D = -0.648 \ln(Re) + 6.21 \tag{44}$$

5.4. Variation in function of the flexibility

Relationship C_D/C_{D0} (α) vs Cauchy Number, Model 1

Taking into consideration the expressions and variables used in model 1 and the Drag coefficients for rigid bodies given in 5.2.2, Table 14 and Figure 54 show the variation of the parameter $\alpha = C_D/C_{D0}$, as a function of the Cauchy number.

Table 14 relationship between C_D and C_{D0} – Model 1

	C_D	C_{D0}	α
White t2	1.67	1.7	1.00
White t2	1.33	1.4	0.96
White t2	1.26	1.2	1.03
Black t1.5	1.62	1.7	0.97
Black t1.5	1.34	1.4	0.98
Black t1.5	1.22	1.2	0.99
Blue t1	1.67	1.7	1.00
Blue t1	1.34	1.4	0.98
Blue t1	1.24	1.2	1.01

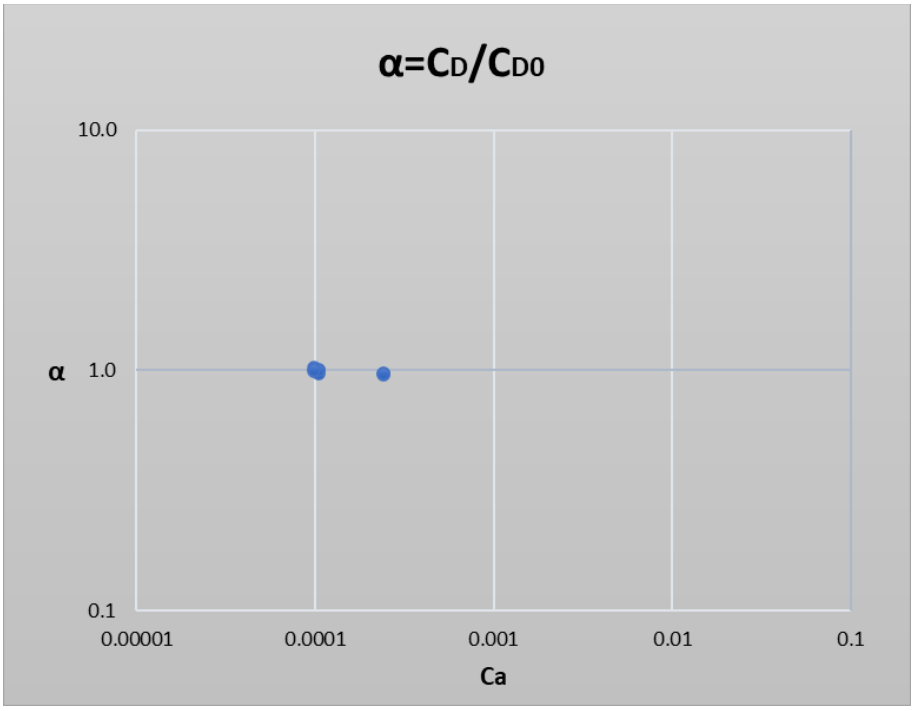

Figure 54 Relationship $\alpha=C_D/C_{D0}$ vs Cauchy Number

When the values are plotted on a larger scale, it is observed that for the range of the Cauchy number (10^{-4} - 10^{-3}), the values of α_b are around 1, this coincides with what was stated by other authors. In Figure 55 it is observed that the relation between C_D and C_{D0} starts to vary significantly from Cauchy numbers greater than 1.

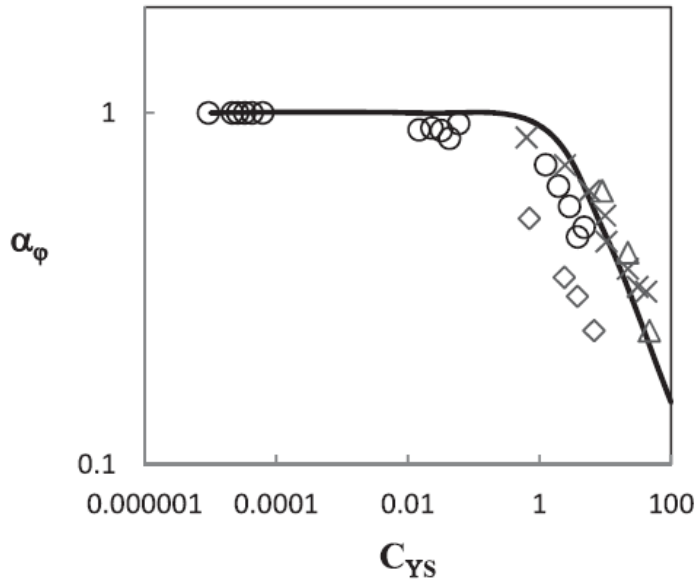

Figure 55 Relationship C_D/C_{D0} vs Cauchy Number (Chapman, Wilson, & Gulliver, 2015)

Relationship C_D/C_{D0} (Rn) vs Cauchy Number: Model 2

In the same way, using the parameters of model 2, for the Cauchy Number range of the current research the reconfiguration number Rn, that also displays the ratio of C_D and C_{D0}, has values less and close to 1.

Table 15 Reconfiguration number - model 2

Obstacle	C_D	C_{D0}	Rn
White t2	1.66	1.78	0.93
White t2	1.32	1.55	0.85
White t2	1.26	1.45	0.87
Black t1.5	1.62	1.78	0.91
Black t1.5	1.34	1.55	0.86
Black t1.5	1.21	1.45	0.84
Blue t1	1.66	1.78	0.93
Blue t1	1.34	1.55	0.86
Blue t1	1.24	1.45	0.85

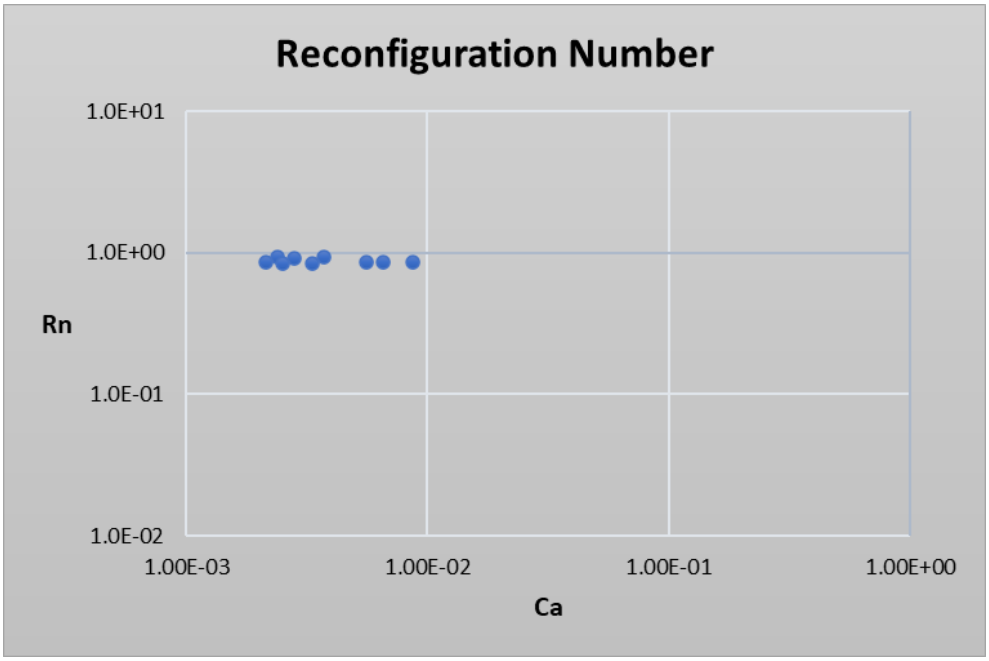

Figure 56 Reconfiguration number vs Ca

It is observed that in previous studies, for the Cauchy number range less than 10^{-2}, the Rn values coincide with those obtained in this dissertation, very close to 1.

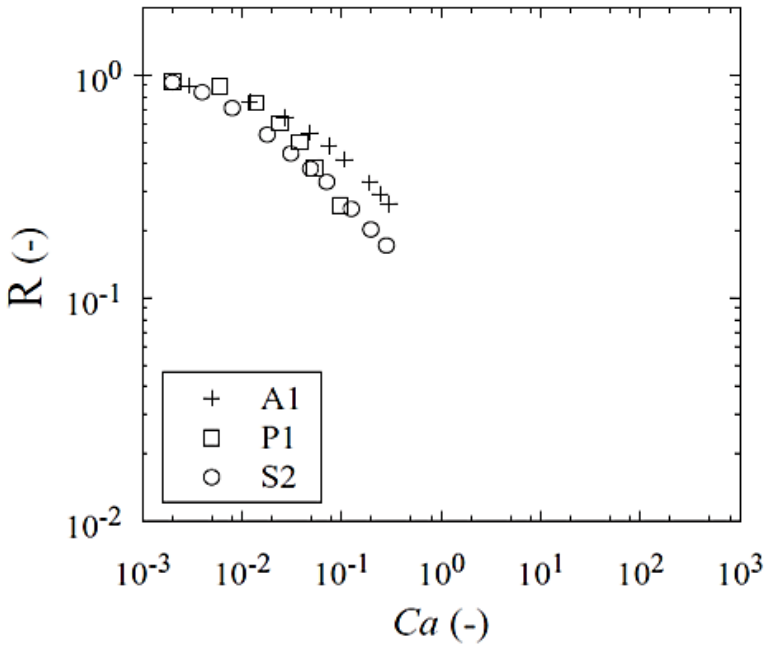

Figure 57 Reconfiguration number vs Ca. Produced from (Whittaker, Wilson, & Aberle, 2015)

Although both models present some variations in the calculation of the drag coefficient and incorporate their own parameters, the relationship between C_D and C_{D0} is very similar, and for our range of Re and Ca, this relationship remains close to 1 in both models.

- **Drag Coefficients by type of cylinder and by velocity**

Below we observe the results obtained in more detail, classifying the values according to the type of obstacle and according to the velocity of the flow. Figure 58 shows the clustered C_D for the three cases studied.

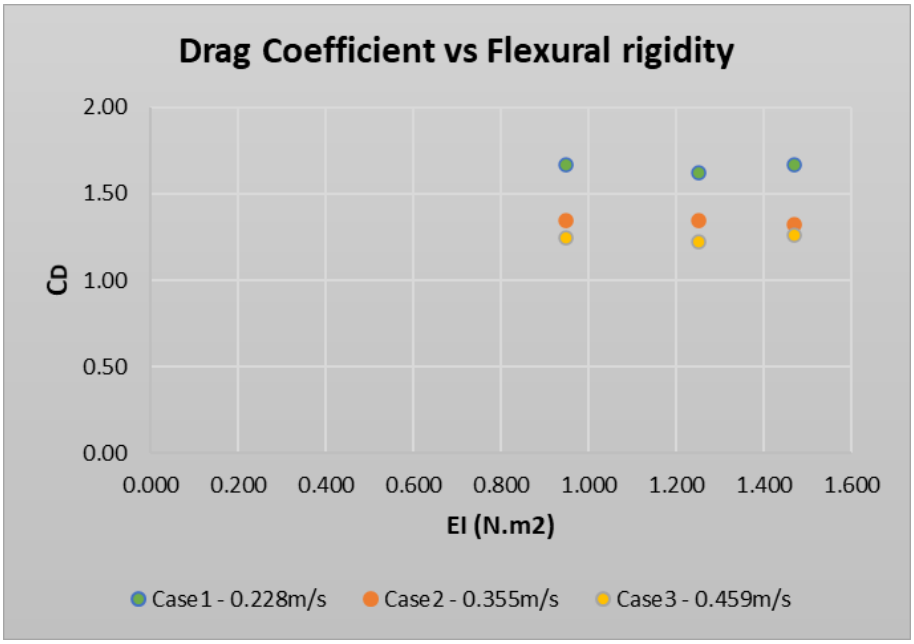

Figure 58 Drag coefficient vs EI - Cases 1, 2 and 3

Although, in general, it is observed that for each case, the C_D values are substantially similar, a slight increase in the drag coefficient can be seen when the obstacles are more rigid, that is, they have greater bending stiffness EI.

The case where this relationship does not take place is the case 2, where we see a slight decrease in the C_D for the stiffer obstacle. This may be due to the fact that, as discussed in section 3.3.1, the flow height oscillated during the tests, which did not happen in cases 1

and 3. However, the difference between this variation and the trends of the other two cases is very small and is part of the dispersion observed in works from most authors.

Figure 59 shows the drag coefficients vs. Reynolds number, grouped according to the type of obstacle.

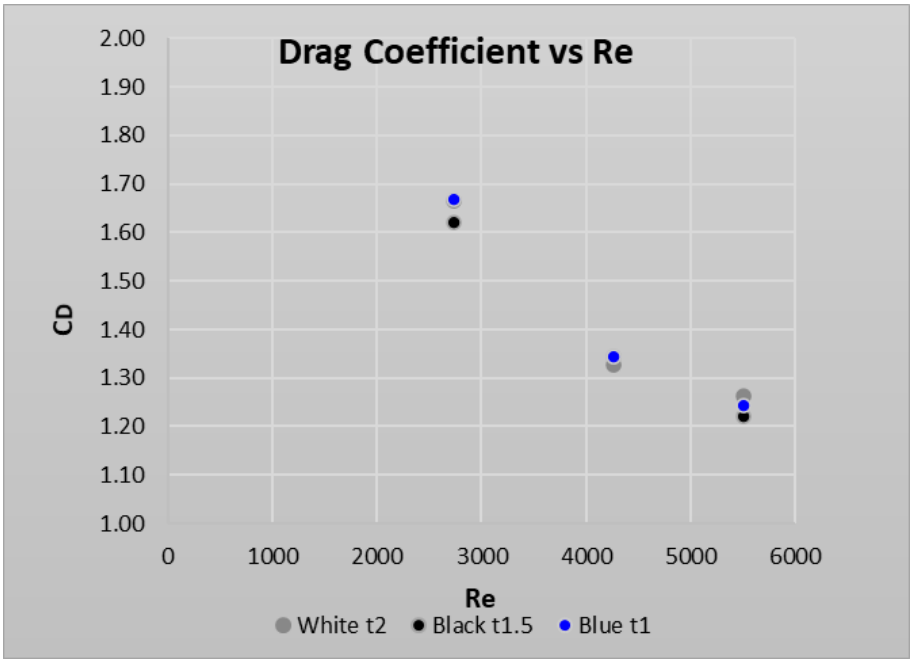

Figure 59 Drag coefficient vs Re - Type of obstacle

The three obstacles follow the Reynolds number dependence studied in Section 5.3, with slight variations due to its rigidity.

6. CONCLUSIONS AND RECOMMENDATIONS

6.1. Conclusions

In this dissertation, we have studied the drag forces in flexible elements, that represent different elements such as vegetation and some man-made structures such as river defences and even larger architectural structures. The model established for this study is based on laboratory experiments of isolated cylinders of three different stiffnesses in three types of uniform flows.

The laboratory experiments were carried out with three types of flows, the Reynolds Number range was from 2000 to 6000. The tested obstacles had Cauchy numbers based on their flexural stiffness in the range from 10^{-3} to 10^{-2}.

With the forces obtained in the laboratory experiments, the drag coefficients were calculated using two models, both based on the states and parameters of Vogel (1984). The model 1 given by Chapman (2015) includes the modulus of elasticity and the slenderness factor to determine the Cauchy number; it also includes an important factor that relates the exposed areas without flow and with flow conditions. On the other hand, the model exposed by Whittaker (2015), where the Cauchy number is also affected by the second moment of area of the obstacle cross-section. Through both models, particularly similar drag coefficients are obtained, with values between 1.2 and 1.7, which agree with those found by the mentioned authors for the same range of Re and Ca.

Model 2 presented here provides a more predictable alternative because it does not rely on a reference velocity required in Model 1, and that is defined in the experiments. Model 2, on the other hand, relies on a mechanical feature of the obstacle as the elastic modulus, which is unfortunately not always easily available for natural obstacles like vegetation.

The forces obtained in the experiments show a relationship with the velocity and flexibility according to expectations. For flexible elements, the relationship varies as identified by Vogel, through the Vogel number ψ, and which can be expected to be $\psi < 0$. For this study, we get $\psi = -0.4 < 0$.

Regarding the experimental forces, the standard deviation σ is strongly affected by the velocity for all stiffnesses. We could demonstrate that σ is greater when the velocity increases.

The relationship of the drag coefficient with the Reynolds number was verified. It is clearly observed that for higher values of Re, we obtained lower values of C_D. For this study, a logarithmic expression is obtained that relates both parameters.

Furthermore, we found that for our range of Cauchy Number, that characterizes the flexibility of the element, the ratio of the determined C_D to the drag coefficient of a rigid element is

around 1. For the highest Ca, this ratio decreases slightly to around 97%; nevertheless, we see that in previous studies, this ratio decreases considerably when the Ca is greater than 1 when it is calculated with the modulus of elasticity, or greater than 10^{-2} when it is calculated with the flexural stiffness.

6.2. Recommendations

The data and dependence relationships studied in this dissertation can be used in a wide field of hydraulic solutions, which involves flexible elements located in the beds and banks of open channels such as rivers, natural and artificial channels. Among these applications, some of the most relevant are:

- Research and analysis of flexible structures as part of flood defences. These structures could be made of some types of trunks or any barrier made of flexible material.
- Reforestation studies of riparian forests for erosion control in flood prevention and management. After determining the amount and types of riparian vegetation that may be used, design considerations can be made depending on the which type of vegetation gives the most advantages in terms of the stability of channel.
- To determine of the right amount of water flow, frequency, and power to kill plants in pest control or due to sanitary reasons.

This dissertation has focused on the study of flexible obstacles, in specific characteristics of the flow and elements. Until now, there is not a single approach that could be used in every scenario. For future studies, it is recommended to vary or combine the properties taking into account the following:

- Expand the Reynolds number range. We have verified in this study the dependence of the drag coefficient on the Reynolds number. It would be significant to verify whether this dependence continues to be a logarithmic function similar to that obtained, testing cylinders in flows of Re smaller than 10^3 and greater than 10^4.
- Expand the range of Cauchy Number. In the present research, we were able to verify that the studied obstacles, even though they are made of a flexible material, their

behaviour does not differ significantly from a rigid obstacle, with only slight reductions in the drag coefficient. While this result has been interesting, to improve the understanding of a greater variety of flexible elements, it is advantageous to study additional objects of different materials and different cross-sections, and verify how they behave for a larger range of Re.

- Obstacle arrays. As we studied in the literature review, obstacle arrays vary the properties of both the flow and the behaviour of the elements. Testing diverse arrays, varying the number of elements, the number of rows, spacing and distribution, it can be developed a better understanding of this topic.
- Obstacle deformations. In this study, the deformations were determined by the finite element method. However, using this method some parameters are assumed and simplified. For future work, the deformations could also be measured in the laboratory to be contrasted with those obtained in the calculations.
- Vibration dependence. The dynamic behaviour of the obstacles is a subject that has not been studied in the present dissertation. There are references from some researchers who found that the relationship between the natural frequency of obstacles and the frequency of the drag force affects the drag coefficient, in some cases finding values up to three times higher than expected. This study is especially relevant to carry out on obstacles with high slenderness ratios.

REFERENCES

Aberle, J., & Järvelä, J. (2013). Flow resistance of emergent rigid and flexible floodplain vegetation. *Journal of hydraulic research*, 33-45.

Albayrak, I., Nikora, V., Miler, O., & O'Hare, M. (2011). Flow-plant interactions at a leaf scale: effects of leaf shape, serration, roughness and flexural rigidity. *Aquatic Sciences*, 267–286.

Alexander, D. (1997). The Study of Natural Disasters, 1977-97: Some Reflections on a Changing Field of Knowledge. *Disasters*, 284-304.

Blaikie, P. (1985). *The political economy of soil erosion in developing countries.* London: Longman.

Chapman, J. A., Wilson, B. N., & Gulliver, J. S. (2015). Drag force parameters of rigid and flexible vegetal elements. *Water Resources Research*, 3292–3302.

Chaudhry, M. H. (2008). *Open-Channel Flow.*

Chen, L., Stone, M. C., Acharya, K., & Steinhaus, K. A. (2011). Mechanical analysis for emergent vegetation in. *Journal of Hydraulic Research*, 766-774.

Cheng, N.-S., & Nguyen, H. T. (2011). Hydraulic Radius for Evaluating Resistance Induced by Simulated Emergent Vegetation in Open-Channel Flows. *Journal of Hydraulic Engineering*, 995-1004.

Chow, V. T. (1959). *Open channel hydraulics.* New York.

CRED, C. f. (2015). *Report on Human cost of Natural Disasters. A global perspective.* Brussels.

Darby, S. E. (1999). Effect of Riparian Vegetation on Flow Resistance and Flood Potential. *Journal of Hydraulic Engineering*, 443-454.

Errico, A., Pasquino, V., Maxwald, M., Chirico, G., Solarie, L., & Preti, F. (2018). The effect of flexible vegetation on flow in drainage channels: Estimation of roughness coefficients at the real scale. *Ecological Engineering*, 411–421.

Hamill, L. (2011). *Understanding hydraulics.* Houndmills, Basingstoke: Palgrave.

Hays, W. W. (1981). *Facing Geologic and Hydrologic Hazards: Earth Science. Earth-Science Considerations.* US Geological Survey Professional Paper 1240-B.

Hibbeler, R. (2011). *Mechanics of Materials.*

Ishikawa, Y., Mizuhara, K., & Ashida, S. (2000). Effect of Density of Trees on Drag Exerted on Trees in River Channels. *Journal of Forest Research*, 271-279.

Jonkman, S. N. (2005). Global Perspectives on Loss of Human Life Caused by Floods. *Natural Hazards*, 151-175.

Langre, E. d. (2008). Effects of Wind on Plants. *Annual Review of Fluid Mechanics*, 141-168.

Loboda, A., Karpinski, M., & Bialik, R. (2018). On the Relationship between Aquatic Plant Stem Characteristics and Drag Force: Is a Modeling Application Possible? *Water*, 540.

Luhar, M., & Nepf, H. M. (2011). Flow-induced reconfiguration of buoyant and flexible aquatic vegetation. *Association for the Sciences of Limnology and Oceanography, Inc*, 2003–2017.

Munson, Y. O. (2009). *Fundamentals of Fluid Mechanics* (6th ed.). United States of America: Don Fowley.

Niklas, K. J. (1991). The Elastic Moduli and Mechanics of Populus tremuloides (Salicaceae) Petioles in Bending and Torsion. *American Journal of Botany*, 89-996.

Nikora, V. (2010). Hydrodynamics of Aquatic Ecosystems: An Interface Between Ecology, Biomechanics and Environmental Fluid Mechanics. *River Research and Applications*, 367–384.

Parker, D. (2014). *Floods.* Routledge.

Pasquino, V., Saulino, L., Pelosi, A., Allevato, E., Rita, A., Todaro, L., . . . Chirico, G. (2018). Hydrodynamic behaviour of European black poplar (Populus nigra L.) under coppice management along Mediterranean river ecosystems. *River Research and Applications*, 586-594.

Stephan, U., & Gutknecht, D. (2002). Hydraulic resistance of submerged flexible vegetation. *Journal of Hydrology*, 27-43.

Stone, M. C., Chen, L., Mckay, S. K., Goreham, J., Acharya, K., Fischenich, C., & Stone, A. B. (2011). Bending of Submerged Woody Riparian Vegetation as a Function of Hydraulic Flow Conditions. *River Research and Applications*, 195-205.

Tanino, Y., & Nepf, H. M. (2008). Laboratory Investigation of Mean Drag in a Random Array of Rigid, Emergent Cylinders. *Journal of Hydraulic Engineering*, 34-41.

Vandiver, J. K. (1983). Drag Coefficients of Long Flexible Cylinders. *Offshore Technology Conference.* Houston.

Vogel, S. (1989). Drag and Reconfiguration of Broad Leaves in High Winds. *Journal of Experimental Botany,*, 941-948.

Wallerstein, N. P., Alonso, C. V., Bennett, S. J., & Thorne, C. R. (2002). Surface Wave Forces Acting on Submerged Logs. *Journal of Hydraulic Engineering*, 349-353.

White, F. M. (1991). *Viscous Fluid Flow.* Columbus: McGraw-Hill US Higher Ed USE.

Whittaker, P., Wilson, C. A., & Aberle, J. (2015). An improved Cauchy number approach for predicting the drag and reconfiguration of flexible vegetation. *Advances in Water Resources*, 28–35.

APPENDIX

- Velocity and Forces form the experiments.

APPENDIX

Below is part of the data collected in the laboratory tests. For a better visualization, the graphs show velocities and forces in a random range of 10 seconds.

1 Case 1

Depth Flow

Boundary depth	z1	191.9	mm
Free layer depth	z2	7.7	mm
Flow depth	y	184.2	mm

Velocity

Channel width	B	300	mm
Channel cross-sect	A	0.055	m2
Volume	Vo	1000	lt
time	t	84.81	s
Flow rate	Q	0.012	m3/s
Velocity	V	0.213	m/s
Mean velocity ADV	Vm	0.228	m/s

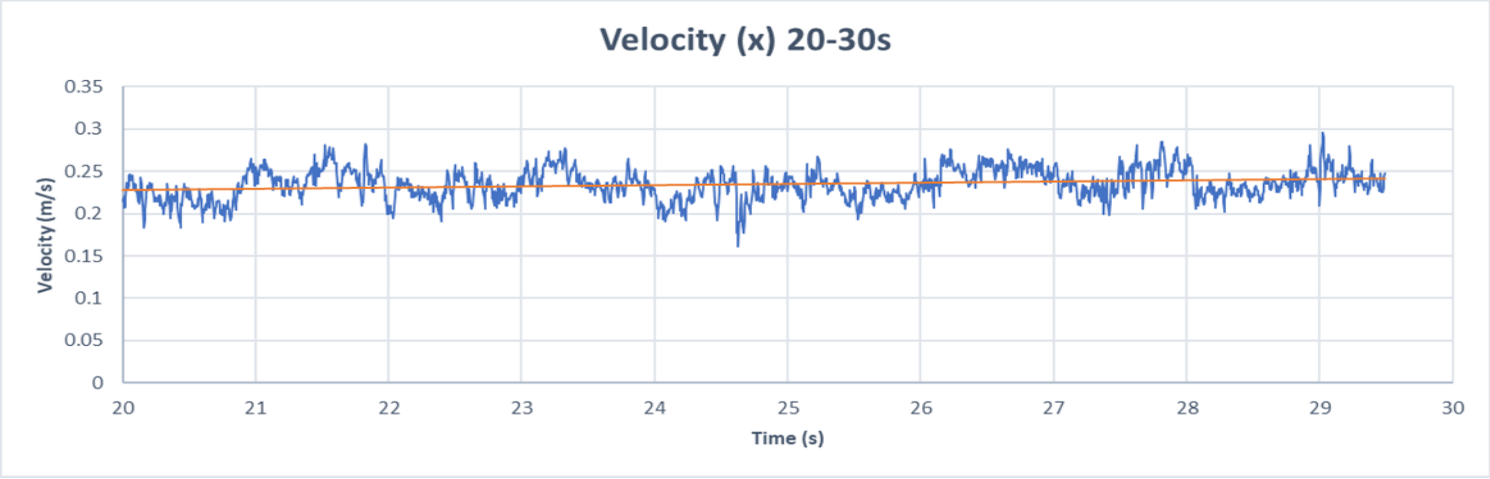

Velocity output - case 1- t=20 to t=30

1.1 ***Obstacle 1 - White***

Radius 1	r1	6	mm
Radius 2	r4	4	mm
Modulus of Elasticity	E_3	1800	N/mm2
Thikness	t_3	2	mm
Height	H	250	mm
Area	Ai	0.0001	m2
Second moment Area	Iyi	8.2E-10	m4

Average force	$F_{D(W1)}$	-0.086	N
Maximun force	$F1_{(W1)}$	0.658	N
Minimun force	$F2_{(W1)}$	-0.709	N

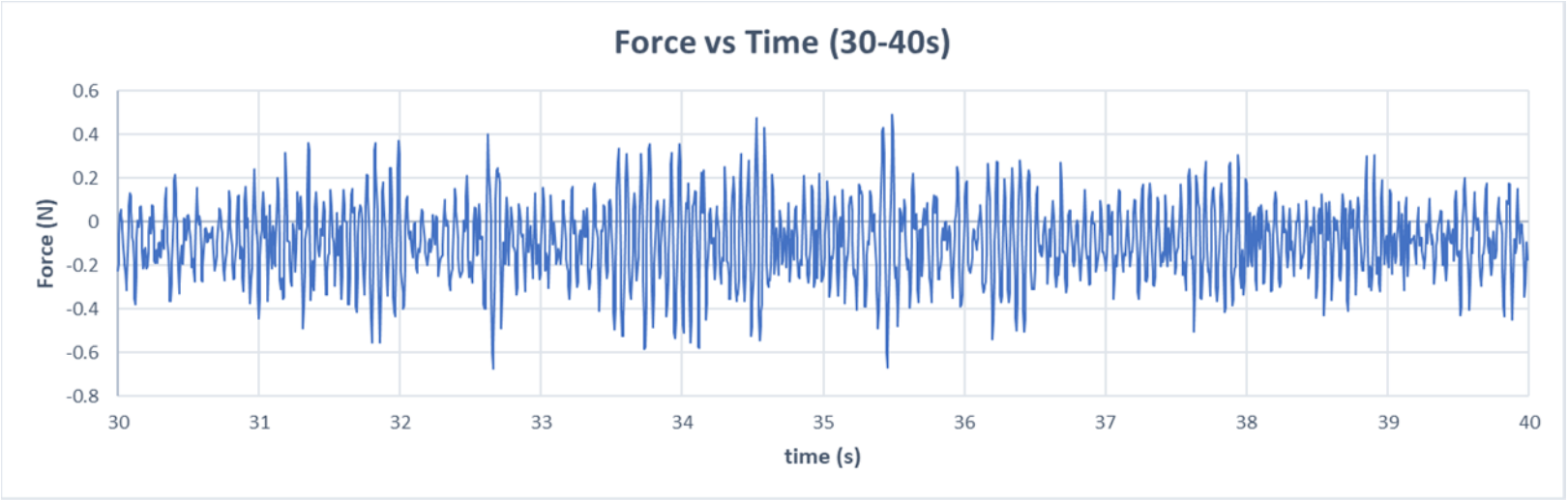

Force output - case 1- Obstacle 1 - t=30 to t=40

1.2 ***Obstacle 2 - Black***

Radius 1	r1	6	mm
Radius 2	r3	4.5	mm
Modulus of Elasticity	E2	1800	N/mm2
Thikness	t2	1.5	mm
Height	H	250	mm
Area	Ai	49.4801	mm2
Second moment Area	Iyi	7.0E-10	m4

Average force	$F_{D(W1)}$	-0.084	N
Maximun force	$F1_{(W1)}$	0.604	N
Minimun force	$F2_{(W1)}$	-0.886	N

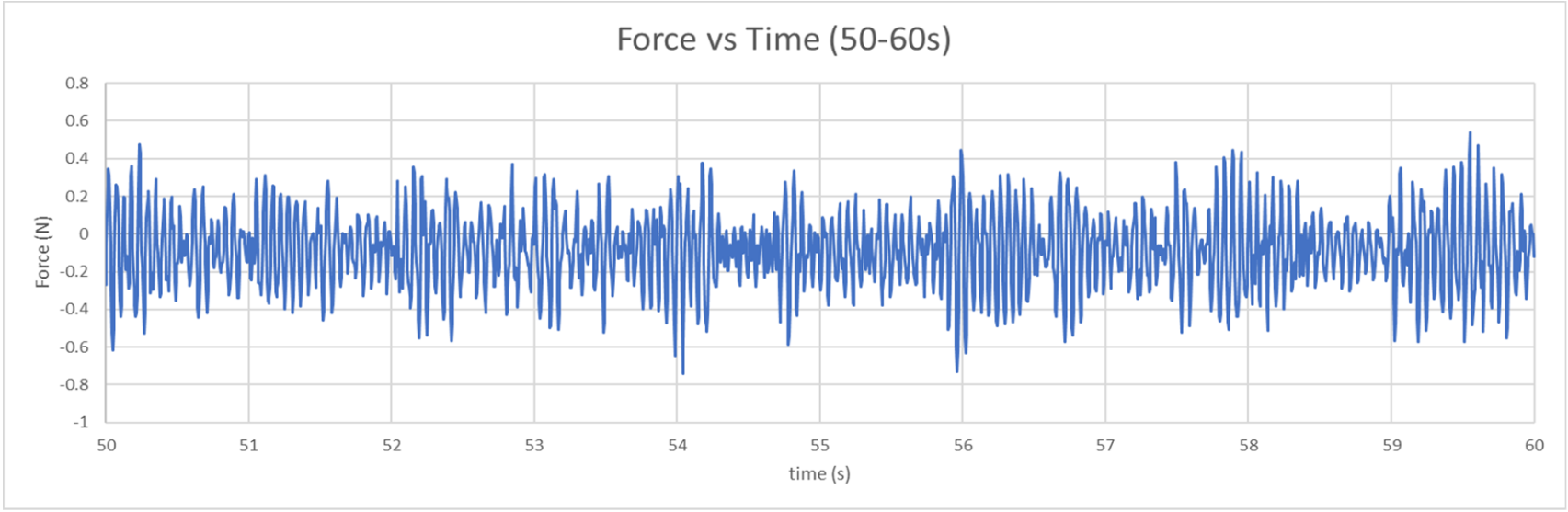

Force output - case 1 - Obstacle 2 - t=50 to t=60

1.3 ***Obstacle 3 - Blue***

Radius 1	r1	6	mm
Radius 2	r2	5	mm
Elasticity Modulus	E_1	1800	N/mm2
Thikness	t_1	1	mm
Height	H	250	mm
Area	Ai	34.56	mm2
Second moment Area	Iyi	5.3E-10	m4

Average force	$F_{D(W1)}$	-0.086	N
Maximun force	$F1_{(W1)}$	0.666	N
Minimun force	$F2_{(W1)}$	-0.811	N

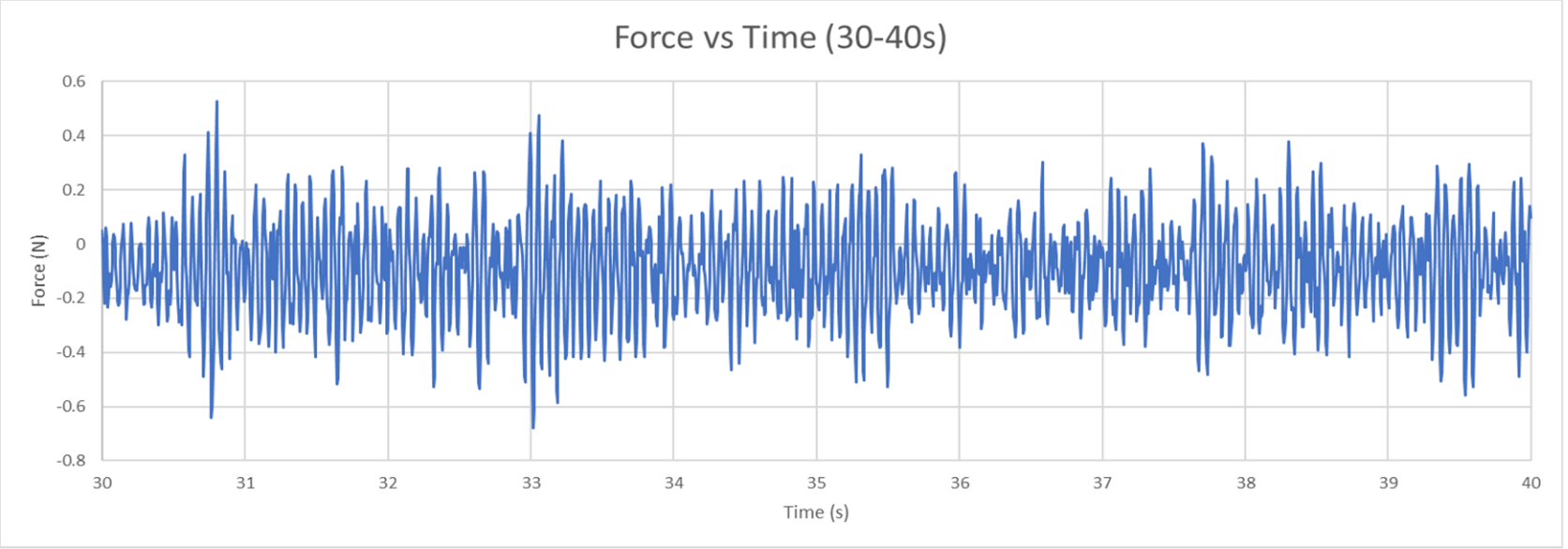

Force output - case 1 - Obstacle 3 - t=30 to t=40

2 Case 2

Depth Flow

Boundary depth	z1	189.6	mm
Free layer depth	z2	7.7	mm
Flow depth	y	181.9	mm

Velocity

Channel width	B	300	mm
Channel cross-sect	A	0.055	m2
Volume	Vo	1000	lt
time	t	51.78	s
Flow rate	Q	0.019	m3/s
Velocity	V	0.354	m/s
Mean velocity ADV	Vm	0.355	m/s

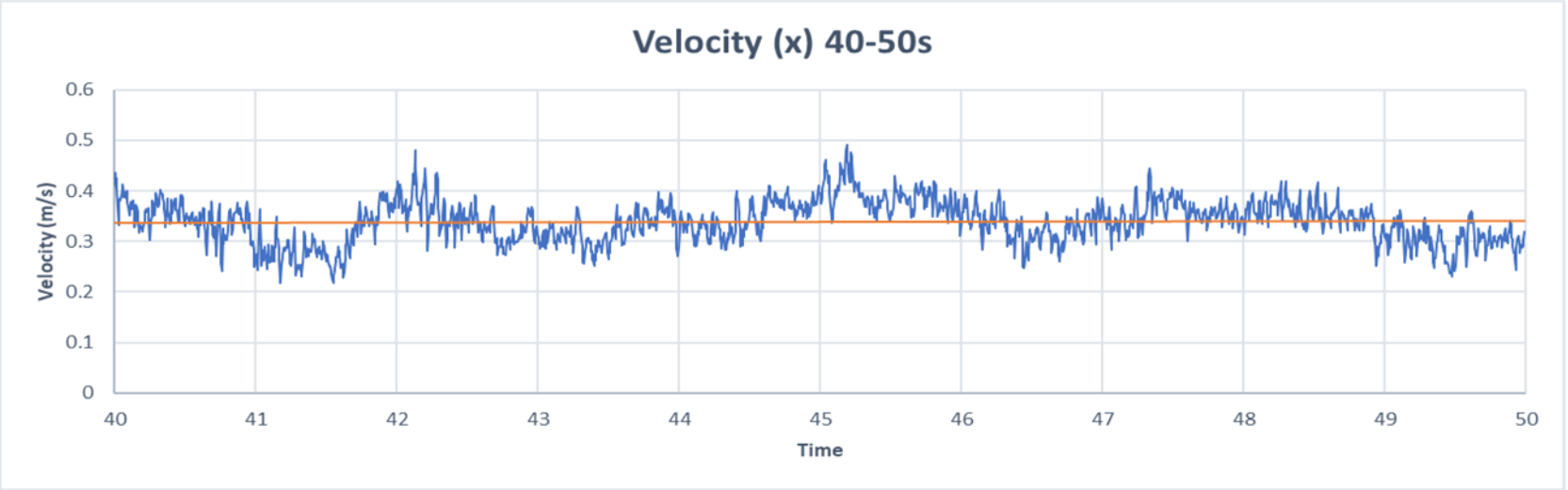

Velocity output - case 2- t=40 to t=50

2.1 ***Obstacle 1 - White***

Average force	$F_{D(W1)}$	-0.164 N
Maximun force	$F1_{(W1)}$	0.628 N
Minimun force	$F2_{(W1)}$	-0.943 N

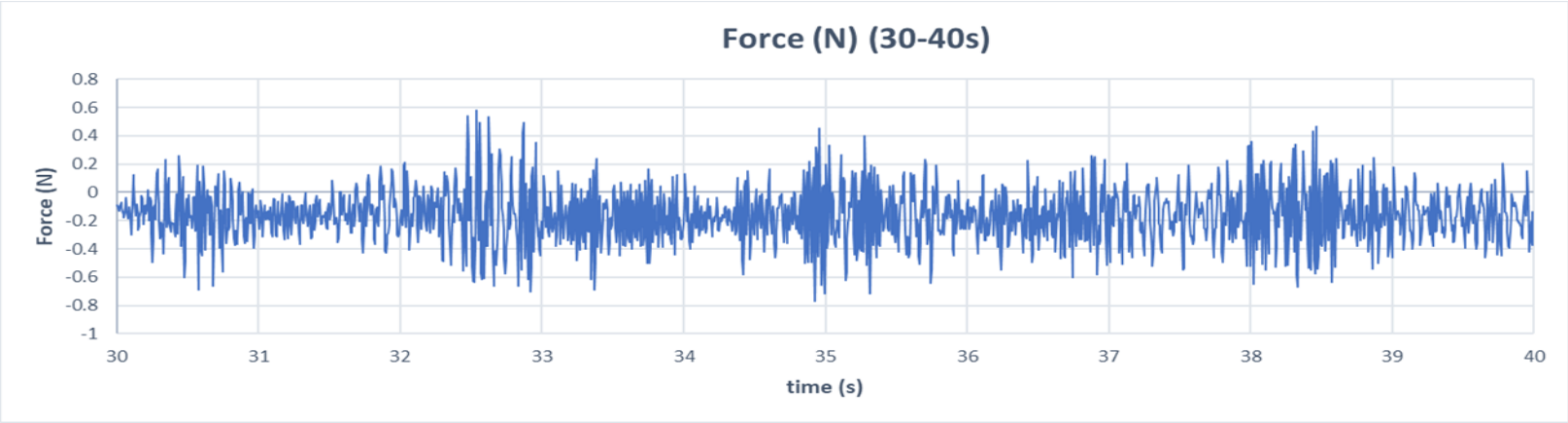

Force output - case 2 - Obstacle 1 - t=30 to t=40

2.2 ***Obstacle 2 - Black***

Average force	$F_{D(W1)}$	-0.166 N
Maximun force	$F1_{(W1)}$	0.693 N
Minimun force	$F2_{(W1)}$	-1.002 N

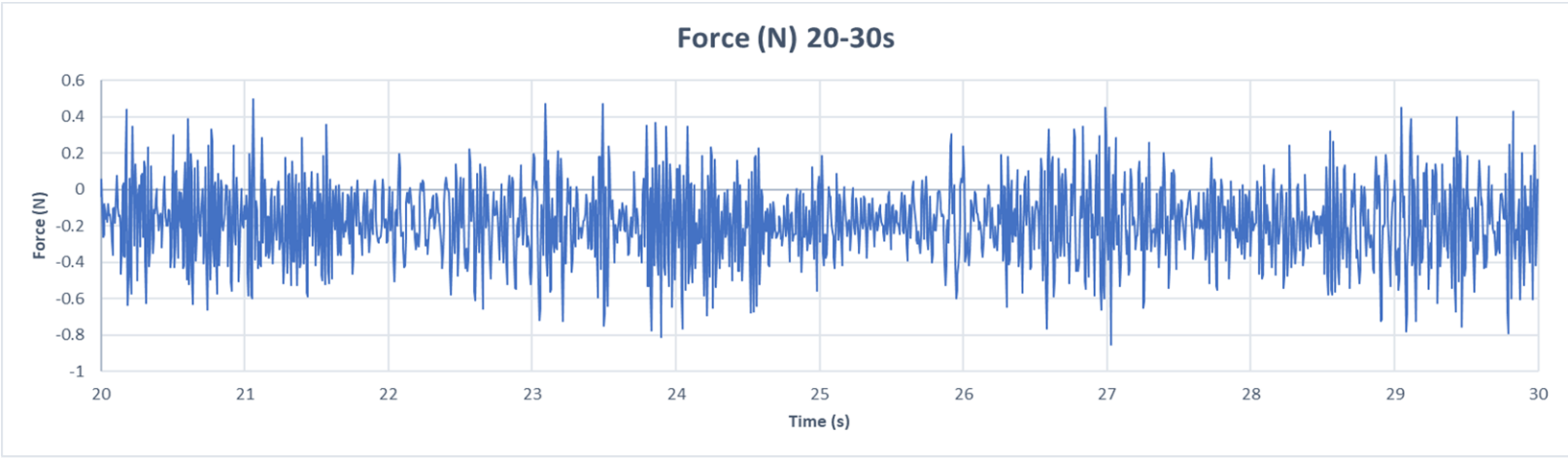

Force output - case 2 - Obstacle 2 - t=20 to t=30

2.3 *Obstacle 3 - Blue*

Average force	$F_{D(W1)}$	-0.166 N
Maximun force	$F1_{(W1)}$	0.693 N
Minimun force	$F2_{(W1)}$	-1.029 N

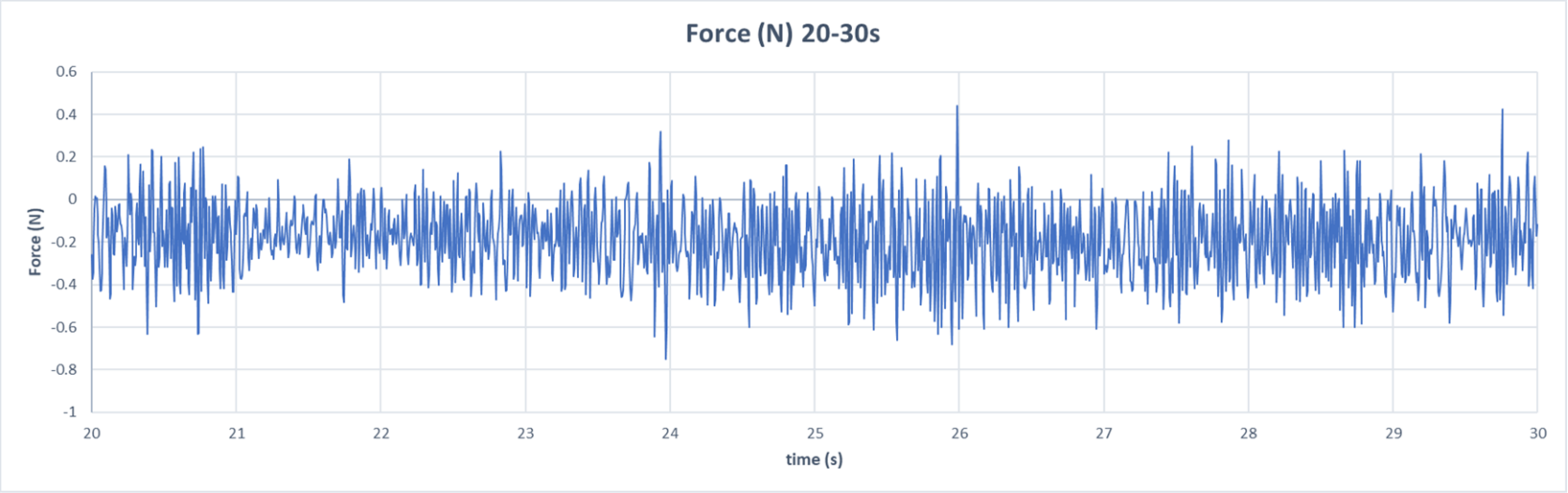

Force output - case 2 - Obstacle 3 - t=20 to t=30

3 Case 3

Depth Flow

Boundary depth	z1	121.4	mm
Free layer depth	z2	7.7	mm
Flow depth	y	113.7	mm

Velocity

Channel width	B	300	mm
Channel cross-sect	A	0.034	m2
Volume	Vo	1000	lt
time	t	68.78	s
Flow rate	Q	0.015	m3/s
Velocity	V	0.426	m/s
Mean velocity ADV	Vm	0.459	m/s

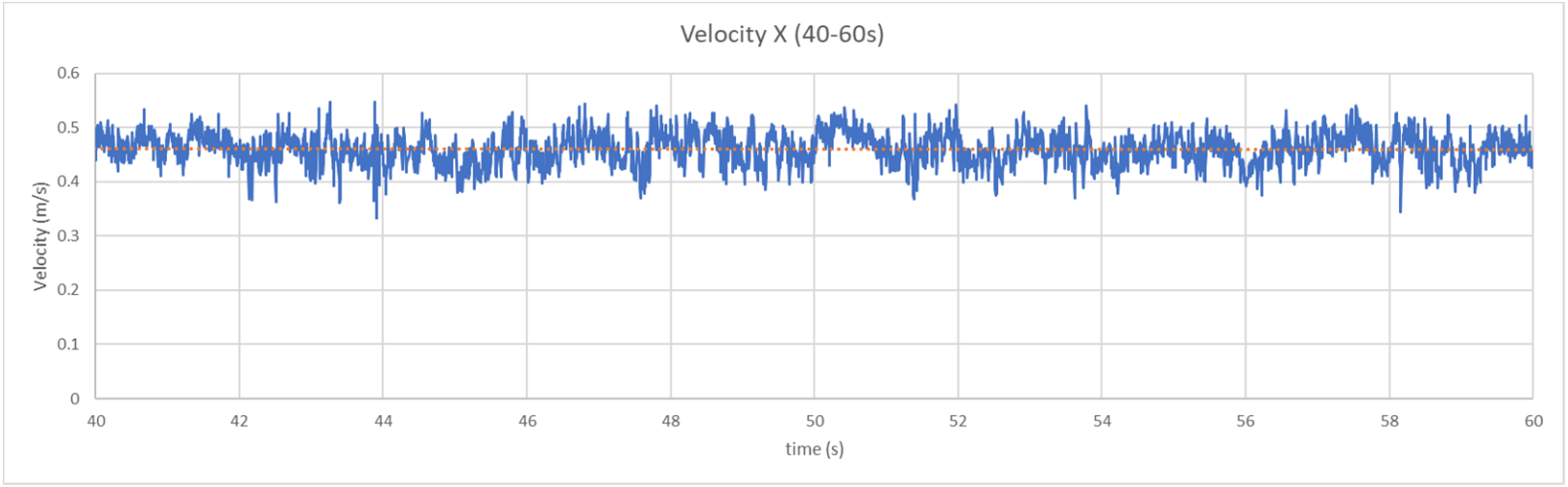

Velocity output - case 3- t=40 to t=60

3.1 *Obstacle 1 - White*

Average force	$F_{D(W1)}$	-0.153 N
Maximun force	$F1_{(W1)}$	0.598 N
Minimun force	$F2_{(W1)}$	-0.862 N

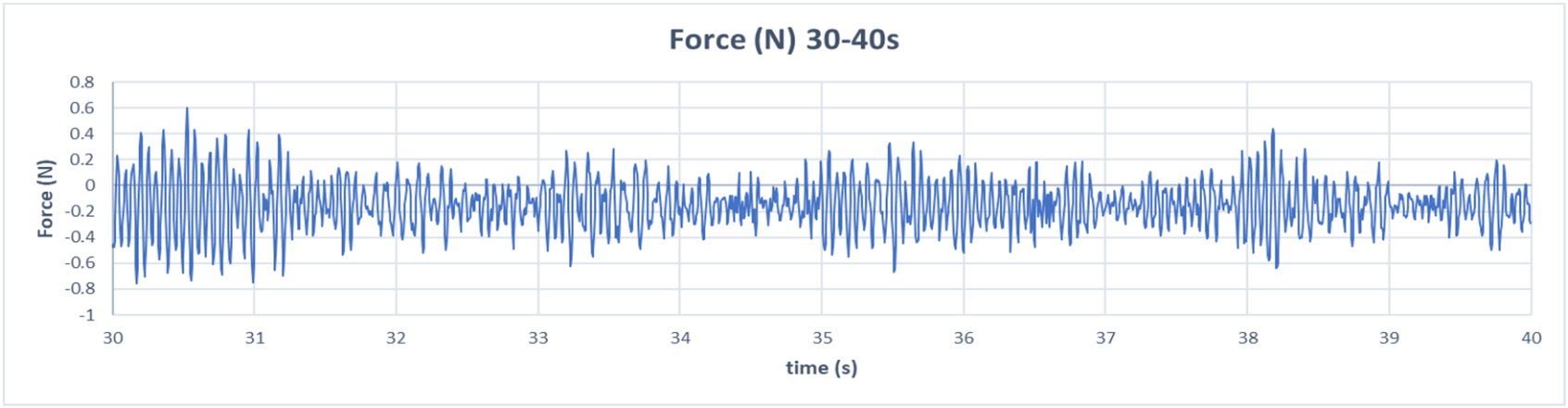

Force output - case 3 - Obstacle 1 - t=30 to t=40

3.2 *Obstacle 2 - Black*

Average force	$F_{D(W1)}$	-0.147 N
Maximun force	$F1_{(W1)}$	0.668 N
Minimun force	$F2_{(W1)}$	-0.881 N

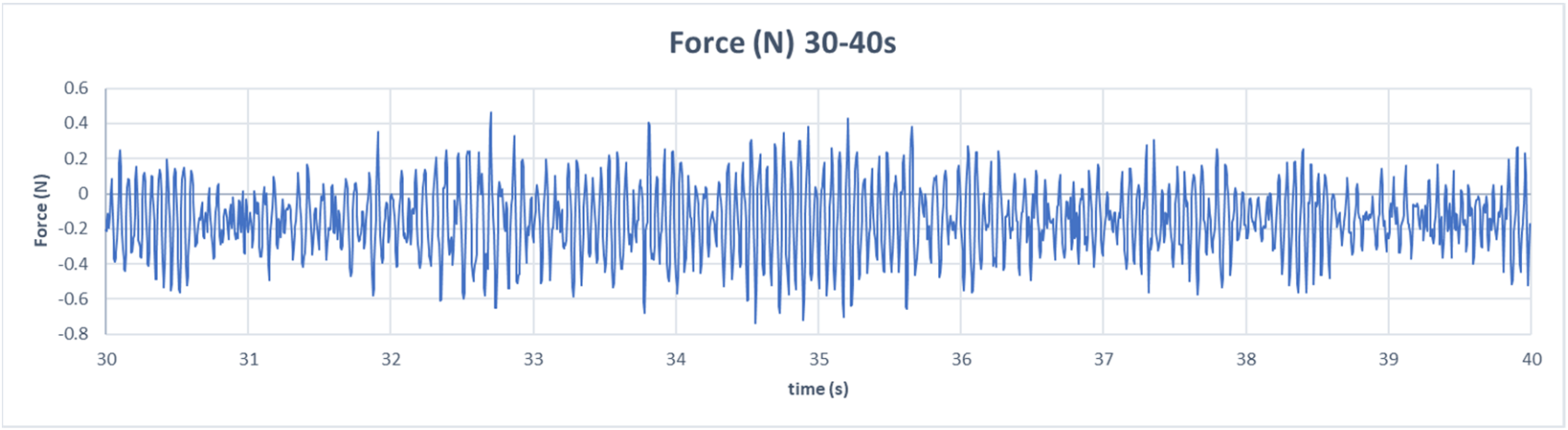

Force output - case 3 - Obstacle 2 - t=30 to t=40

3.3 *Obstacle 3 - Blue*

Average force	$F_{D(W1)}$	-0.150 N
Maximun force	$F1_{(W1)}$	0.544 N
Minimun force	$F2_{(W1)}$	-0.870 N

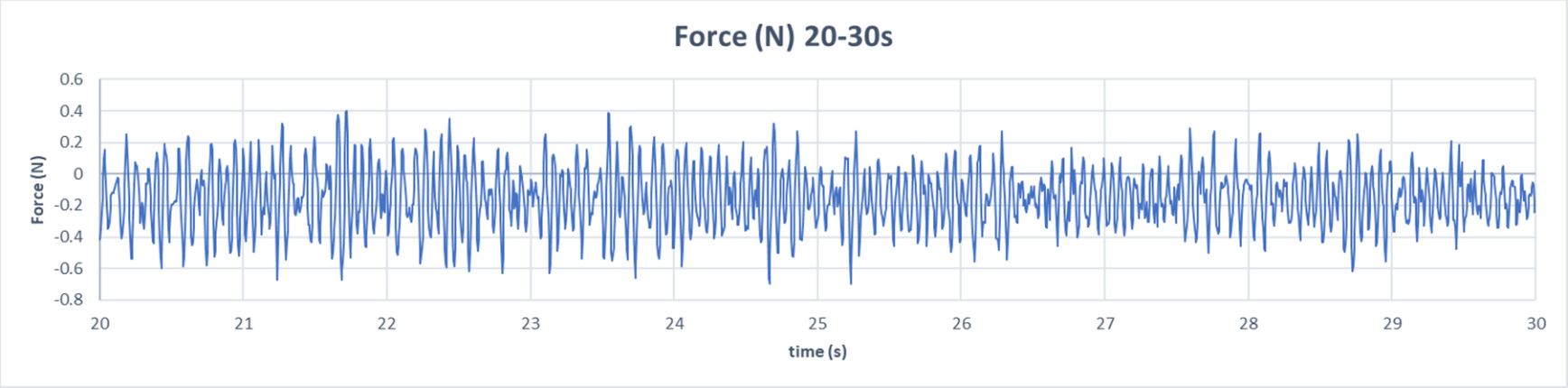

Force output - case 3 - Obstacle 3 - t=20 to t=30